Reduction of resonance frequency with magneto-dielectrics, for UHF microstrip antennas

Emanuel Rygg

Thesis submitted for the degree of
Master in Robotics and Intelligent Systems
60 credits

Department of Technology Systems
Faculty of mathematics and natural sciences

UNIVERSITY OF OSLO

Autumn 2022

Reduction of resonance frequency with magneto-dielectrics, for UHF microstrip antennas

Emanuel Rygg

Reduction of resonance frequency with magneto-dielectrics, for UHF microstrip antennas

http://www.duo.uio.no/

Printed: Reprosentralen, University of Oslo

Abstract

The antenna dimensions are determined by the length of the intended resonating wavelength. However, there exist methods to achieve miniaturization, and material-based miniaturization with magneto-dielectrics is one such method. Its potential for use in miniaturization is expanding, as new materials are made available, and these new materials can be divided into natural magneto-dielectric materials and artificial metamaterials.

A 7.1 cm wide square microstrip antenna with an air-filled substrate, was designed as a reference antenna. This antenna was then redesigned to include MagTrex 555 as a magneto-dielectric substrate. The simulations showed a gain of 0.8 dBi and a 4.0% -10 dB impedance bandwidth when the ground was set to half a wavelength. Measurements confirmed that a majority of the energy was absorbed as magnetic losses, and the antenna realized a 76.6% reduction of the natural resonance frequency.

The antenna was then modified a second time, but this time with a metamaterial made from C-ring resonators. The simulations show a resonance at 1.07 GHz, which is a 50.7% reduction of the resonance frequency. The simulated -10 dB impedance bandwidth was 7.5%, and the maximum directivity was 5.4 dBi, even with a small ground. The simulated reduction of the resonance frequency was confirmed with a 2.8% accuracy from measurements. The antenna was then measured in an anechoic chamber which realized a maximum gain of 2.3 dBi at 0.983 GHz. The measurements had poor impedance matching, due to the small patch dimension. Matching was improved by changing to a capacitively coupled feed, which achieved a radiation efficiency of 55% and a -10 dB impedance bandwidth at 10%. It might be possible to improve gain even further, if the ground plane were enlarged to half a wavelength.

Magneto-dielectric materials offer miniaturization without compromising the bandwidth, and a high directivity is achieved when the ground plane is sufficiently large. The chosen natural magneto-dielectric materials resulted in high magnetic losses and a large weight, which restricts some of its potential use cases. On the other hand, the metamaterial antenna proved its potential for tailored miniaturization, but it require a high accuracy in the design and manufacturing process, to maximize its potential.

Contents

List of Figures

List of Tables

Chapter 1

Preface

This thesis was submitted for the degree of Master of Science (M. Sc), in Robotics and Intelligent Systems at the Department of Technology Systems at the University of Oslo.

The idea for the thesis came during earlier employment, where I was introduced to ferrite rod antennas for VHF (Very High Frequency) communication. The bachelor's degree was finalized already in 2008, but the work with this master's thesis has been carried out part-time during employment at FFI, from January 2021 to November 2022 under the supervision of Associate Professor Terje Tjelta and Professor Johannes Skaar. I would like to thank my supervisors for their patience and insight, which have been essential to realizing the thesis. The prototypes were manufactured with the help of the Department engineer Pål Grønstad Solheim. FFI has financed most of the expenses and provided valuable input through Ph. D. Karina Viera Hoel.

Chapter 2

Introduction

Since the invention of radio communication, more complex communications systems have been gradually developed, including systems with high bit rates and intricate antenna designs. The dimensions of the antennas are determined by the physical length of the resonating wavelength. This has resulted in VLF (Very Low Frequency at 3 to 30 kHz) antennas being stretched between mountain tops and constraints on the movement of tactical vehicles with VHF (Very High Frequency at 30 to 300 MHz) antennas. Whenever there is a physical limitation for antennas, they are often miniaturized. Miniaturization is achieved when a small antenna is made able to resonate at the same wavelengths as a larger antenna. Widespread examples of miniaturized antennas are meander wire and loop antennas, and both these achieve resonance at the cost of reduced gain and bandwidth. What if miniaturization could be achieved with reduced negative effects on the antenna parameters by manipulating the propagation of the electromagnetic wave?

An electromagnetic wave propagates at the speed of light. In a denser medium, such as air, the phase velocity of light is slower than in a vacuum. This relative phase velocity in a medium or material is due to its magnetic and dielectric properties. Materials such as this are already being utilized for radio communication at the cost of degrading the bandwidth and gain. However, the recent development of new materials with reduced loss may give hope for higher antenna performance.

The potential applications for miniaturized antennas are endless, but the added complexity does often degrade their performance. A potential for miniaturization of antennas is in the UHF (Ultra High Frequency at 300 MHz to 3 GHz) range and lower bands. This is when the antenna dimension is challenging to integrate into handheld devices, man packs, vehicles and satellites. The thesis investigates material-based miniaturization with magneto-dielectrics, and how the material can be effectively utilized to reduce the resonant frequency, which could allow the design of smaller antennas to resonate at larger wavelengths. Multiple designs were tested with simulations before the most promising ones were verified with measurements. The designs have not targeted any specific communications system but instead focused on the techniques and their

potential.

The background presents the antenna parameters and their physical bounds, natural magneto-dielectric materials, metamaterials and the design process for a microstrip antenna. The two following chapters contain, firstly, the design and analysis of a microstrip antenna with a commercially available magneto-dielectric substrate and then equally with a metamaterial. Finally, the metamaterial antenna is taken to an anechoic chamber for measurements. The parameters of focus are the reduction of resonance frequency, bandwidth, radiation efficiency, directivity and gain. The thesis ends with a description of challenges, future work and a conclusion.

2.1 Methods used to reduce the resonant frequency

An infinite number of possible antenna designs exist, but they all contain dimensions that electrically match a fraction of the intended wavelength. There are multiple methods to reduce physical dimensions while still maintaining the necessary electrical length. When the physical dimension is reduced, the antennas tend to be less efficient and dissipate their excess energy as heat, which results in degraded radiation efficiency. One approach categorizes them as topology- and material-based miniaturization (Fallahpour and Zoughi, 2018), as described in a review in IEEE Antennas and Propagation Magazine.

2.1.1 Topology based

The topology-based method optimizes the geometry of an antenna to achieve the desired radiation characteristics while reducing the overall dimension (Fallahpour and Zoughi, 2018). The overall dimension is reduced when the radiating elements are curved to fill a larger part of an already reduced space. Typical examples of antennas with such space-filling curves are the meander and fractal antennas. They are known for their low manufacturing cost and significant size reduction. However, they do not offer any high gain since the currents at the adjacent conducting curves are out of phase and tend to cancel each other's respective radiation in the far field.

2.1.2 Material based

The material-based method encompasses the techniques which are slowing the wave propagation in the near field, and consequently, decreasing the guided wavelength. Popular techniques to achieve this is through dielectrics, magnetics and combined through magneto-dielectric materials. The material-based method is very suitable for microstrip antennas since their physical size is inversely proportional to the effective refractive index of the substrate, as the antenna is considered a loaded cavity resonator (Fallahpour and Zoughi, 2018).

Dielectrics

A higher permittivity for the substrate results in a slower wave propagation inside the resonator and, consequently a lower resonant frequency for its dominant mode (Fallahpour and Zoughi, 2018). Using such a material as a substrate will reduce its radiation efficiency due to the excitation of surface waves, energy storage as an electric field, and dielectric loss. A high dielectric substrate will affect the intrinsic impedance of the antenna and can result in difficulties in impedance matching and reduced bandwidth.

Magnetics

A popular utilization of magnetics for miniaturization is when loop antennas with ferrite rods are implemented into AM (Amplitude Modulation) home radios. Balanis (2005) explains how these loop stick antennas are very poor radiators and are seldom used in the transmitting mode. They are instead used to receive signals, such as in radios and pagers, where the signal-to-noise-ratio is much more important than efficiency (Balanis, 2005). The radiation resistance of a loop stick antenna is usually negligible compared to the loss resistance, where its total losses are due to losses in rod, copper and electromagnetic coupling between the rod and the adjacent conductive parts (Snelling, 1969). The magnetic rod loss is the sum of the hysteresis loss, eddy current loss and a residual loss component (Fujita, Kobiki and Gotoh, 1998). The losses are dissipated as heat, which for high-power applications, can degrade the magnetic properties of the ferrite. The magnetic losses are described with the imaginary permeability, which becomes dominant at higher frequencies.

New materials with high permeability and low loss have been investigated for application in antennas. One finding was that substrates with high real permeability do not decrease the antenna bandwidth, contradictory to materials with high real permittivity (Hansen and Burke, 2000). They suggested instead that a high real permeability relative to the real permittivity can reduce the overall losses. However, similarly to a dielectric antenna, the magnetic material can result in difficulties during antenna matching.

Natural magneto-dielectrics

An alternative to dielectric and magnetic substrates is substrates which combine both these properties. With similar values of magnetic and dielectric properties, the intrinsic impedance of a substrate is matched to the intrinsic impedance of air (Fallahpour and Zoughi, 2018). This reduces the need for a matching network and can contribute to achieving a reduction of resonance frequency with improved radiation efficiency and bandwidth. Combined substrates were earlier realized by stacking magnetic and dielectric substrates together, but this made them bulky, lossy and anisotropic (Fallahpour and Zoughi, 2018). However, recent research has offered new materials with promising electromagnetic properties for utilization for DVB-T (Terrestrial Digital Video Broadcasting) at 200 MHz

(Bae et al., 2009) (Li et al., 2019) (Mathur et al., 2010) (Kim et al., 2014). A number of these studies have been focused on the sintering of the materials, measurement of their properties and simulation of how they affect an antenna. It seems to be a potential for experimental validation of these studies to truly understand their effect on the antenna parameters.

Artificial magneto-dielectrics / metamaterials

The concept of combining permittivity and permeability was initially introduced by Veselago (1968), and some of these combinations have just recently been made possible through the design of metamaterials. Metamaterials are created with the help of conducting microstructures, with the purpose to affect the performance of antennas. A metamaterial can be integrated into the antenna environment, the antenna structure or as a part of the feeding network.

The effect of a metamaterial substrate on the parameters for a microstrip antenna has been discussed (Kärkkäinen and Ikonen, 2005). It was shown that the frequency dispersion of the substrate plays a vital role for the impedance bandwidth of the antenna. To achieve a high radiation performance and a sufficient impedance bandwidth, the antenna must operate below the divergence frequency of the metamaterial substrate, in the spectral range where there is a weak dispersion of the material characteristics, low loss behaviour, and an acceptable high permeability value (Ikonen et al., 2006).

2.2 Research question

The question which will be investigated is; to what extent are radiation efficiency, bandwidth and directivity affected by matched material-based reduction of resonance frequency, with magneto-dielectrics?

The answers to this question will be searched for in the UHF frequency range, referenced to a microstrip antenna with an air-filled substrate. The width and length of the microstrip antenna will be fixed throughout all the designs. The focus will be on the antenna itself, including impedance matching from the design of the antenna, and the thesis will, therefore not include any external matching network.

Chapter 3

Background

This chapter includes a short presentation of the antenna parameters and their physical bounds. Then the microstrip antenna is presented, and the constitutive parameters and how these parameters are realized with natural magneto-dielectric substrates and artificial metamaterials.

3.1 Antenna parameters

The primary purpose of an antenna is to convert an electrical signal into an electromagnetic wave and vice versa. How well an antenna function is described with the help of antenna parameters.

Scattering

A common approach to explain the loss impedance over a frequency range, is with the help of the scattering parameters (Balanis, 2005).

For every port, there are two scattering parameters. The first parameter (S_{11}) describes the relationship between the incident and reflected power (or voltage) as

$$S_{11} = \frac{P_{\text{reflected}}}{P_{\text{incident}}} = \Gamma. \tag{3.1}$$

The reflections can also be expressed with $VSWR$ (Voltage Standing Wave Ratio) as

$$VSWR = \frac{1+\Gamma}{1-\Gamma}. \tag{3.2}$$

The second scattering parameter (S_{21}) describes the relationship between transmitted and incident power (or voltage), were

$$S_{21} = \frac{P_{\text{transmitted}}}{P_{\text{incident}}}. \tag{3.3}$$

3.1.1 Bandwidth

The bandwidth is the width of the frequency band that is accepted by the system. Depending on the purpose of the system, there are multiple

approaches to defining what is considered to be accepted. One popular approach is the -10 dB impedance bandwidth, which is the frequency band where 90% of the power delivered to the feed is accepted by the system (Balanis, 2005). The -10 dB impedance bandwidth can be extracted from a plot of the S_{11} scattering parameter. This bandwidth can alternatively be expressed with the quality (Q) factor, which, relative to the centre frequency (f_c) indicate how narrow the bandwidth is, with

$$BW = \frac{f_c}{Q} \text{ [Hz]}. \tag{3.4}$$

Mclean (McLean, 1996) proposed an equation for finding the quality factor for electrically small antennas. He suggests that the quality factor is calculated with the help of the propagation constant k and the diameter of the minimum enclosing sphere of the antenna (a), where

$$Q = \frac{1}{(ka)^3} + \frac{1}{ka}. \tag{3.5}$$

A reduced enclosing sphere will, according to this, require a proportionally increase of the propagation constant k to ensure a low quality factor.

Wavelength and propagation constant

The propagation constant k is found from the wavelength, were

$$k = \frac{2\pi}{\lambda} \text{ [rad m}^{-1}\text{]}. \tag{3.6}$$

The wavelength is the distance a wave will travel before it repeats itself. Hence, the wavelength within a medium is found from the frequency when the refractive index (n) is taken into consideration through

$$\lambda = \frac{c}{nf} \text{ [m]}. \tag{3.7}$$

3.1.2 Directivity

The directivity is the maximum radiation intensity in the desired direction to the average radiation intensity in all other directions (Balanis, 2005), written as

$$D = 4\pi \frac{U(\omega, \phi)}{P_{\text{radiated}}}, \tag{3.8}$$

where U represent the power per unit solid angle. The directivity is dimensionless and usually expressed in decibels relative to an isotropic radiator (dBi), where an isotropic radiator radiates equally in all directions. This also allows the directivity to be expressed with the help of the maximum (dB) and average (dB) scattering parameters S_{21} as

$$D = S_{21\text{maximum}} - S_{21\text{average}} \text{ [dB]}. \tag{3.9}$$

The directivity of a microstrip antenna is calculated from the width of the patch (W) and the current (I_1). The directivity of a single-slot microstrip antenna may be expressed as (Balanis, 2005)

$$D = \frac{2\pi W^2}{\lambda} \frac{1}{I_1}. \tag{3.10}$$

Where the current (I_1) is found with Equation 3.31, and it indicates that a maximized width is necessary to ensure maximum directivity.

3.1.3 Radiation efficiency

In addition to the direction, an important concern is how large amount of the energy is radiated. For a given input voltage or current, the radiation efficiency is expressed as the radiation impedance relative to the total impedance, as

$$\eta = \frac{Z_{\text{radiated}}}{Z_{\text{radiated}} + Z_{\text{loss}}}. \tag{3.11}$$

The loss impedance is related to the overall efficiency (e_0) of the antenna. The overall efficiency is the product of the reflection efficiency (e_r), conduction efficiency (e_c) and dielectric (and magnetic) (e_d) efficiency (Balanis, 2005), from

$$e_0 = e_r e_c e_d. \tag{3.12}$$

The radiation efficiency (η) is utilized to describe the radiated power from an antenna (P_{radiated}). The radiated power is the product of the incident power (P_{incident}) and the radiation efficiency, and is expressed as

$$P_{\text{radiated}} = \eta P_{\text{incident}} \text{ [W]}. \tag{3.13}$$

Wheeler's cap method

Radiation efficiency is usually measured in an anechoic chamber with a transmitting and a receiving antenna. An alternative approach to finding the radiation efficiency was proposed by Wheeler (Quiterio, 2004), as illustrated in Figure 3.1. The radiation efficiency was in Equation 3.11, described as the relationship between transmitted and incident power. The incident power is found with an S_{11} plot, when the antenna is positioned in free space, without any obstacles in the near field. This allows power to leave the antenna as radiation. Then another S_{11} plot is created, but this time with a reflecting cap around the antenna, which ensures reflection of all power that is not dissipated as heat. Based on these two plots, it is possible to calculate how much energy is absorbed as heat and then the radiation efficiency of the antenna. A way to express this is with $VSWR$, as

$$\eta = 1 - \frac{VSWR^{fs}}{VSWR^{wc}}. \tag{3.14}$$

The optimum radian length for the cap is λ divided by 2π (Quiterio, 2004).

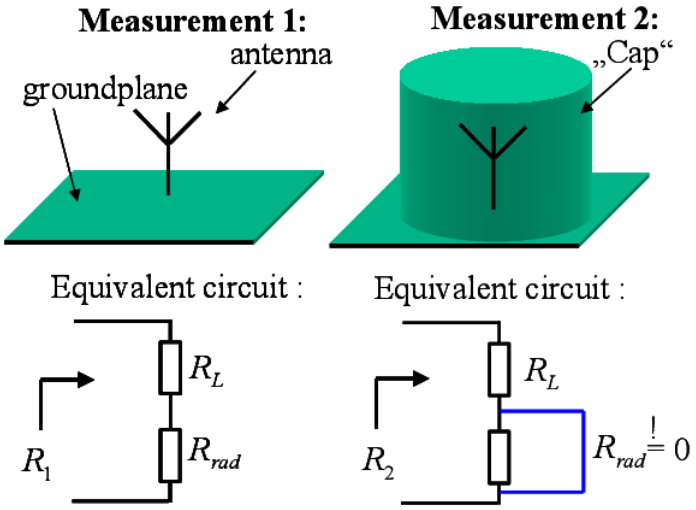

Figure 3.1: Wheeler's cap method (Litschke et al., 2003)

3.1.4 Gain

The gain of an antenna is a measure which combines the radiation efficiency of an antenna with its directional capabilities. Gain is the ratio of the radiation intensity in a given direction to the radiation intensity that would be obtained if the power accepted by the antenna were radiated isotropically (Balanis, 2005). This is expressed as

$$G = \eta D. \tag{3.15}$$

Both the gain and the directivity are described either through their maximum values or with a plot considering all spherical directions. By including the port efficiency, the gain is denoted as realized gain.

3.2 Physical bounds

The antenna performance is a result of the physical limitations of the antenna, and there have been multiple attempts to define these relations.

Chu presented in 1948 the physical limitation of omnidirectional antennas. He analyzed the field of a vertically polarized antenna, and based on its radiation characteristics; he made an expression for both the maximum gain ($G(\infty)_{\max}$) and the minimum quality factor. Since he realized their interdependence, he also proposed an equation for the maximum gain to quality-factor ratio (Chu, 1948). He concluded that the antenna gain was a consequence of the antenna dimension and the wavelength. To obtain a gain higher than this value, the quality factor will have to be increased. He did assume that the antenna was located in a vacuum and did, therefore, not consider the effect of any refractive materials in the near field. He did also assume perfect conditions with a perfectly conducting ground plane, no physical objects nearby and no conduction losses.

Harrington analyzed in 1960 the effect of antenna size on the antenna parameters (Harrington, 1960). If a high gain is desired, the antenna must be a narrow-band device. Also, if the antenna is lossy, the efficiency will fall (Harrington, 1960). Harrington defines the maximum gain in the far zone ($ka \rightarrow \infty$) from the number of modes N, as

$$G(\infty)_{\max} = N^2 + 2N, \tag{3.16}$$

where the number of modes (N) is the product of the propagation constant k and the radius of the minimum enclosing sphere.

Skin depth and far field

The skin depth is how deep into the conductor the electrical wave is travelling at resonance. It is calculated from the square root of the resistivity; (ρ) divided by resonating frequency and magnetic permeability, as

$$\delta = \sqrt{\frac{\rho}{\pi f \mu}} \text{ [m]}. \tag{3.17}$$

This skin depth defines the minimum thickness of the conductors, which is useful both during the simulations and for manufacturing.

The far-field domain is the region outside the near field. even though there is no clear distinction between the near field and the far field. The minimum distance to an approximate end of the near-field region (NFR) is found with the wavelength (λ) and the diameter of a minimum enclosing sphere (a) of the antenna, and is expressed as

$$NFR = \frac{2a^2}{\lambda} \text{ [m]}. \tag{3.18}$$

3.3 Microstrip antenna basics

3.3.1 Lead-up to the choice of antenna type

The first antenna design which was considered for this thesis was the loop stick antenna. This was due to the utilization of magnetic rods to achieve material-based miniaturization of antennas, which commonly are implemented in AM home radios. One challenge with these loop stick antennas is the parallel loops of wire which both should create magnetic fields in the ferrite rod, at the same time as they should not interfere with each other.

On the other hand, a microstrip is considered a loaded cavity resonator, and it seemed like a better approach where the focus could be on the substrate itself. The microstrip antenna does have a rich history, and it exists a plethora of research and practical implementations of these antennas.

3.3.2 Geometry

The microstrip antenna is a nearly two-dimensional structure, which consists of a radiating patch, the ground plane and a space-dividing substrate.

There is a large variety of equations which are utilized in the design of a patch antenna. The utilization of the term height (h) in this thesis will describe the distance between the patch and the ground plane. This distance will, during this work, always be considered filled with a substrate.

A practical approximation for the width of a half-wavelength radiating patch is calculated with the requested centre frequency (f_c) and the relative permittivity (Balanis, 2005), as

$$W = \frac{1}{2f_c}\sqrt{\frac{2}{\epsilon_r + 1}}\ [\mathrm{m}]. \tag{3.19}$$

The microstrip dimensions are dependent on the constitutive parameters. There have been multiple attempts to predict these dependencies, but they have focused explicitly on a microstrip separated from the ground by a dielectricum. Hammerstad modified Schneider's equations and adjusted them to achieve higher accuracy. According to Hammerstad, the initial effective permittivity is calculated from the width and height (Hammerstad, 1975) as

$$\epsilon_{\mathrm{eff}} = \frac{\epsilon_r + 1}{2} + \frac{\epsilon_r - 1}{2}\frac{1}{\sqrt{1 + 12\frac{h}{W}}}\ [\mathrm{F\,m^{-1}}]. \tag{3.20}$$

While the dimensions of the patch are finite along the length and width, the edges of the patch will undergo fringing (Balanis, 2005). This fringing edge effect is represented as a normalized length extension, where its dependency to the height has been reduced by Hammerstad from Silvester and Benedek (Hammerstad, 1975). The effect of fringing is found from the width, height and effective permittivity, where

$$\frac{\Delta L}{h} = 0.412\frac{\epsilon_{\mathrm{eff}} + 0.3}{\epsilon_{\mathrm{eff}} - 0.258}\frac{\frac{W}{h} + 0.262}{\frac{W}{h} + 0.813)}). \tag{3.21}$$

The electrical length will, due to fringing, be larger than the physical length of the patch. The electrical length is found by subtracting the length extensions at each side of the patch, as

$$L_{\mathrm{fringed}} = W - 2\Delta L\ [\mathrm{m}]. \tag{3.22}$$

This thesis will focus on a square microstrip antenna, but the fringing fields will, according to Hammerstad, add a length extension which contributes to the reduction of the resonance frequency.

Ground plane dimension

The minimum dimensions for the ground plane to ensure a high gain and low losses are found (Balanis, 2005), by

$$W_g = 6h + W \text{ [m]}, \tag{3.23}$$

and

$$L_g = 6h + L \text{ [m]}. \tag{3.24}$$

The patch is normally half a wavelength which requires the ground to be even larger than this. However, when the antennas have their resonance frequency reduced while keeping the physical antenna dimension, the ground plane can end up being even smaller than half a wavelength, which would result in poor directivity.

3.3.3 Impedance matching with feed

Microstrip antennas with a reduced patch or increased height, end up having its capacitance reduced, since

$$C = \epsilon \frac{A}{d} \text{ [F]}, \tag{3.25}$$

where the antenna impedance is the sum of all contributions as

$$Z_{\text{tot}} = R - \frac{1}{j2\pi fC} + j2\pi fL \text{ [}\Omega\text{]}, \tag{3.26}$$

including the inductivity

$$L = \frac{\mu N^2 A}{l} \text{ [H]} \tag{3.27}$$

which usually is zero. A large permittivity would counteract the effect of a reduced patch dimension, which is the case for antennas with a dielectric substrate. Alternatively, an antenna with a reduced patch dimension could be matched with a large permeability. However, this may result in a mismatch between the impedance of the near field and the intrinsic impedance of the far field, as described by Equation 3.46.

Another approach is to utilize the reactive properties of a feed to perform the remaining impedance matching. There are numerous known techniques to feed the antenna, and each technique has its advantages and disadvantages in terms of bandwidth, complexity and impedance. Four common feed techniques are (Balanis, 2005);

- Line (inset) feed
- Probe feed
- Coupled feed
- Aperture feed

Line (inset) feeds are easy to fabricate since they can be etched or cut out of the patch material, and there is no need for soldering or making holes in the

substrate. It is simple to match by controlling the inset position and width. The line (inset) and probe feeds are inductive, while the aperture and coupled feeds are capacitive. The coupled feed has the largest bandwidth, is easy to model, and has low spurious radiation, but its fabrication is more challenging (Balanis, 2005).

Inset width

Hammerstad presented in 1975 an equation for the relationship between the width and height of a transmission line with a known impedance. It contains an improvement of the constant B_1 in Wheeler's synthesis equation, where it is now

$$\frac{w_f}{h} = \frac{2}{\pi}\{B_1 - 1 - \ln(2B_1 - 1) + \frac{\epsilon_r - 1}{2\epsilon_r}\left[\ln(B_1 - 1) + 0.39 - \frac{0.61}{\epsilon_r}\right]\}, \tag{3.28}$$

and the constant B_1 now represents;

$$B_1 = \frac{\eta\pi}{2\sqrt{e_r}Z}. \tag{3.29}$$

An inset feed is expected to be very wide, according to Equation 3.28 when utilized for antennas of large height. A probe feed does not have this problem (Balanis, 2005) and has low spurious radiation. However, it also has a narrow bandwidth and is more difficult to model.

Feed depth

The patch itself is expected to have a large impedance at its radiating ends and zero impedance in the middle. Hence to match the transmission line impedance, the patch will have to be fed at the correct position, which usually is the position which has 50 $[\Omega]$ impedance. The feed depth for a microstrip antenna is found with the help of the conductances (G_1 and G_{12}) (Balanis, 2005).

With knowledge of the current, the input conductance of a single slot is calculated as

$$G_1 = \frac{I_1}{120\pi^2}\ [\text{S}]. \tag{3.30}$$

The current (I_1) itself is found from the width (W) and the propagation constant k, where

$$I_1 = \int_0^\pi \left[\frac{\sin(\frac{kW}{2}cos\theta)}{\cos\theta}\right]^2 \sin^3\theta\, d\theta\ \ [\text{A}], \tag{3.31}$$

and the mutual conductance (G_{12}) is found from

$$G_{12} = \frac{1}{120\pi^2}\int_0^\pi \left[\frac{\sin(\frac{kW}{2}\cos\theta)}{cos\theta}\right]^2 J_0(kL\sin\theta)\sin^3\theta\, d\theta\ \ [\text{S}]. \tag{3.32}$$

The feed depth (y_0) is then calculated with the help of these conductance's and the requested matched incident resistance (R_{incident}), as

$$R_{\text{incident}} = \frac{1}{2(G_1 + G_{12})} = 50 \cos^2 \frac{\pi}{L} y_0 \ [\Omega]. \tag{3.33}$$

3.4 Constitutive parameters

The constitutive parameters describe the relationship between the flux densities and the field intensities. The constitutive parameters define together the refractive index, as the square root product of the relative electric permittivity (ϵ_r) and the relative magnetic permeability (μ_r), were

$$n = \sqrt{\mu_r \epsilon_r}. \tag{3.34}$$

Veselago (1968) proposed a coordinate system to classify materials based on the sign of permittivity and permeability. He describes how the propagation of an electromagnetic wave is determined by the sign of the permittivity and permeability at different frequencies. An elaborate version of the coordinate system is shown in Figure 3.2.

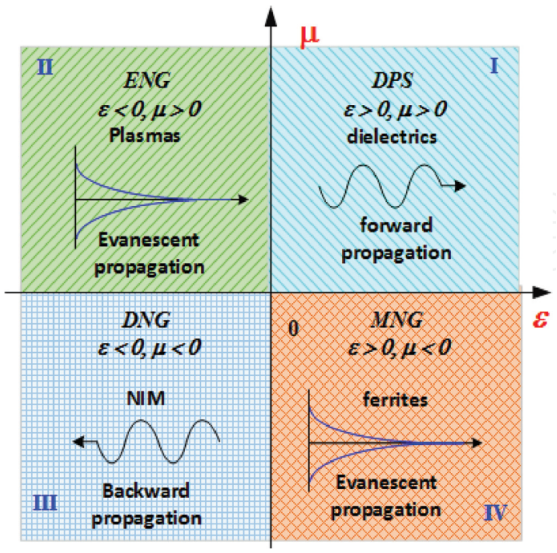

Figure 3.2: Classification of electromagnetic materials (Krzysztofik and Cao, 2019)

Magnetic permeability

The first component is magnetic permeability. The magnetic permeability is the resistance factor of a material against the formation of a magnetic flux density (B) when exposed to changes in magnetic field intensity (H), were;

$$B = \mu H \ [\text{Wb m}^{-1}]. \tag{3.35}$$

The magnetic permeability is often written relative to the absolute permeability of vacuum (μ_0), which is $4\pi \times 10^{-7}\mathrm{H\,m^{-1}}$, where

$$\mu = \mu_0 \mu_r \ [\mathrm{H\,m^{-1}}]. \tag{3.36}$$

Electric permittivity

The second component is electric permittivity. Electric permittivity is the capacity of the material to polarize. The electric field intensity (E) and the electric flux density (D) are related through the electric permittivity, where

$$D = \epsilon E \ [\mathrm{C\,m^{-1}}]. \tag{3.37}$$

The electric permittivity is often written relative to the absolute permittivity of vacuum (ϵ_0), which is $8.85 \times 10^{-12}\mathrm{F\,m^{-1}}$, where

$$\epsilon = \epsilon_r \epsilon_0 \ [\mathrm{F\,m^{-1}}]. \tag{3.38}$$

3.5 Effect of magneto-dielectric materials on the antenna performance

A dielectric and magnetic material within the near field, could affect the propagation of the nearby electromagnetic waves. Due to hysteresis, the radiated power from the antenna will be reduced, which also may affect the bandwidth of the antenna.

3.5.1 Radiated power and loss

The radiated power was presented in Equation 3.13, whereas Equations 3.11 and 3.12 suggested that the reduction in radiation efficiency was due to conductive, dielectric and reflection losses. The dielectric losses do, in this case, also encompass other refractive losses, such as magnetic losses. The overall losses for an antenna, besides the reflection losses, are expressed as (Balanis, 2005);

$$P_{\mathrm{loss}} = P_m + P_d + P_r \ [\mathrm{W}]. \tag{3.39}$$

The substrate power losses are expressed with the help of the loss tangents, the width of the substrate, the height of the substrate and the electric field amplitude (E_0) (Niamien et al., 2011), as

$$P_d = \frac{1}{2}(E_0)^2 \frac{Wh \tan\delta_\epsilon}{240} \sqrt{\frac{\epsilon_r}{\mu_r}} \ [\mathrm{W}], \tag{3.40}$$

and the magnetic power loss as

$$P_m = \frac{1}{2}(E_0)^2 \frac{Wh \tan\delta_\mu}{240} \sqrt{\frac{\epsilon_r}{\mu_r}} \ [\mathrm{W}]. \tag{3.41}$$

Where the dielectric loss tangent is defined as

$$\tan\delta_\epsilon = \frac{\omega\epsilon'' + \sigma}{\omega\epsilon'}, \tag{3.42}$$

and the magnetic loss tangents as

$$\tan \delta_\mu = \frac{\omega \mu^{''} + \sigma}{\omega \mu^{'}}. \tag{3.43}$$

The equations suggest that a high real permittivity increases the losses, while a high real permeability decreases the losses. It may be tempting to conclude that a large substrate height should be avoided based on the equations, but the electric field amplitude is dependent on the height, which leaves the width to be the driving dimension for the electromagnetic substrate losses.

3.5.2 Bandwidth

There have been multiple attempts to predict how a refractive substrate affects the maximum bandwidth of an antenna. One equation was developed by Niamien, and takes the height (h), width (W), radiation conductance (G_r) and the loss tangents of the substrate into account (Niamien et al., 2011), where

$$BW = \frac{1}{\sqrt{2}} \left(240 \frac{h}{W} G_r \sqrt{\frac{\mu_r}{\epsilon_r}} + \tan \delta_\epsilon + \tan \delta_\mu \right) \ [\%]. \tag{3.44}$$

The equation suggests that large height, wide substrate and large loss tangents would widen the bandwidth of the substrate.

3.6 Realizing magneto-dielectrics with metamaterials

The term metamaterial was coined by Walser at The University of Texas in 1999 as macroscopic composites, having synthetic, three-dimensional, periodic cellular architecture designed to produce an optimized combination which is not available in nature, of two or more responses to a specific excitation (Walser, 2003). The word metamaterial consists of two words, where meta is Greek and is translated to beyond, and the second word is material. By this composition of words, any material which has characteristics which are beyond those which are found in nature, could be considered metamaterial. Metamaterials are engineered with novel or artificial structures to produce electromagnetic properties that are unusual or difficult to obtain. These structures are usually built by one or more unit cells. A unit cell is a single cell which has an electric or magnetic impedance response to an alternating electric or magnetic field.

The term metamaterial encompasses both structures with a single unit cell and periodical structures of unit cells. They can either be integrated as an active part of the antenna, conducting a current from the feed or passively in the near field of the antenna environment. To maximize induced response to a magnetic field, the cell(s) should be positioned so that the magnetic field from the antenna, induces a surface current at the unit cell(s). Possible positions for a unit cell array are illustrated in Figure 3.3. The ability of the metamaterial to interact with an electromagnetic field

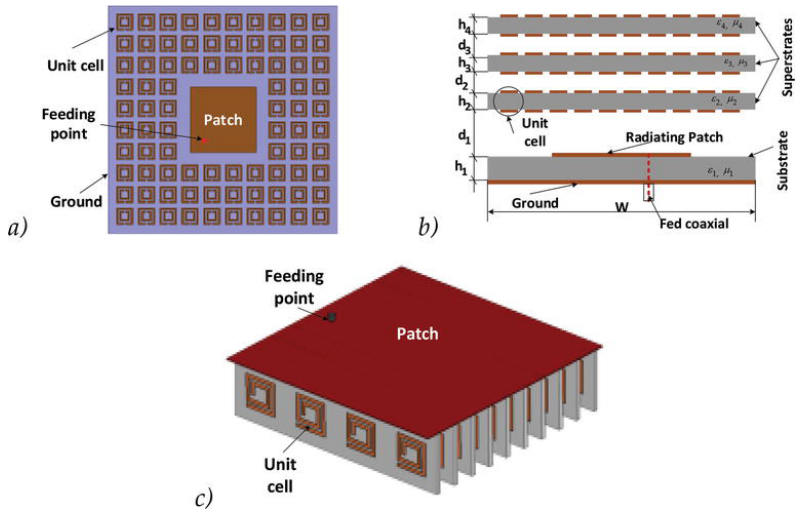

Figure 3.3: How metamaterials can be positioned in antennas: (a) unit cells surrounding the radiated patch, (b) metamaterials as superstrate and (c) using the metamaterials as antenna loading (Krzysztofik and Cao, 2019)

allows it to be utilized for gain improvement, bandwidth enhancement, multi-band creation, or antenna size miniaturization (Krzysztofik and Cao, 2019). A unit-cell array must be under half a wavelength to avoid multiple lobes (Gross, 2011). The total number of unit cells is determined by both the wavelength and the unit-cell dimension. The design of each cell, including its size, shape, orientation and packing density, determines its electromagnetic contribution. A two-dimensional unit cell is expected to have anisotropic properties, which restrict the transmission of electromagnetic waves, dependent on the direction of the unit cell(s).

Unit-cell shape

The unit cells must be large enough to resonate at the intended wavelength, and the thickness is usually under 1/20 of the wavelength (Gross, 2011). Increasing the electric size of the rings decreases the resonant frequency of the resonators and following the antenna up to a certain limit with a minimum allowed return-loss level (Kärkkäinen and Ikonen, 2005). Increasing the packing density has a similar effect. The unit cell acts as a passive filter with both inductive and capacitive properties. A study (Ouedraogo et al., 2012) suggested a radiation efficiency of 28.1% after a 1/16 area reduction, due to the reduced antenna volume.

The simplest design is the C ring, where the circular ring acts as a conductor and allows capacitance to build up in the gap. Two C rings can together form a split ring resonator if they have slightly varying sizes and a gap at opposite sides. The split ring resonator is a well-known unit-cell structure, but other structures promise an even higher reduction of the resonant frequency. A square spiral with multiple turns allows a longer conductor, which results in a smaller unit cell dimension. More complex

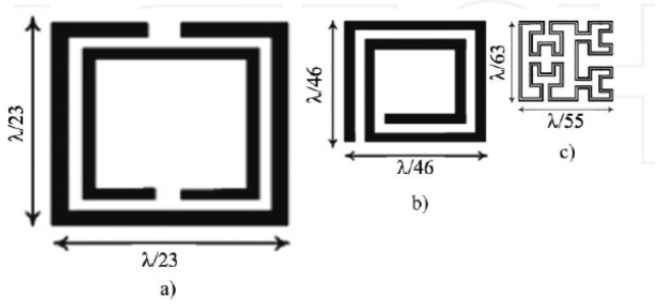

Figure 3.4: Different types of unit cells; (a) a unit cell of inclusion with SRR, (b) square spiral (SSR) and (c) third-order Hilbert fractal (Krzysztofik, 2017)

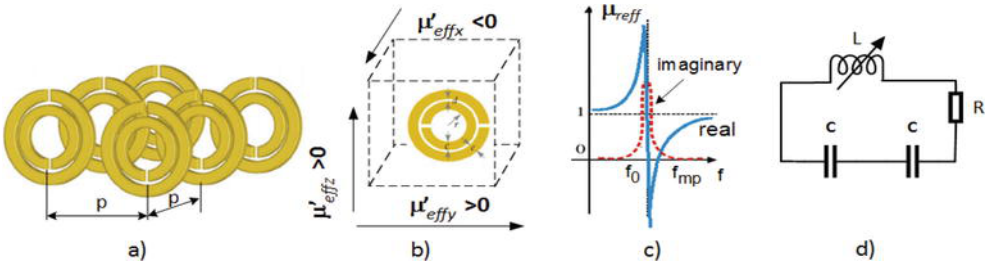

Figure 3.5: An array of SRRs (a), SRR unit cell (b), the effective permeability of SRR array (c), and equivalent circuit (d) (Krzysztofik and Cao, 2019)

structures force the current to move an even further distance, as with the second, third or fourth Fractal Hilbert inclusion. The resonance frequency is highly dependent on the length of the conductor (Krzysztofik and Cao, 2019). Squared structures are easier to fabricate than round structures; hence they are favourable for manufacturing. Some of the possible unit-cell designs are shown in Figure 3.4.

The resonator will act as a band-stop filter where the resonator impedance is the product of the resistance, the inductance from the ring and the capacitance from the gap. Multiple resonators will increase the inductance and add additional capacitance due to their proximity to nearby resonators, which are illustrated in Figure 3.5. Hence the number of cells, their radius, the thickness of the conductor, gap size and distance to other resonators will all contribute to the divergence frequency (f_d), which is calculated as

$$f_d = \frac{1}{2\pi\sqrt{LC}}\ [\text{Hz}]. \tag{3.45}$$

For the electromagnetic wave to move from the near field to the far field of the antenna, the antenna impedance will have to be matched to the intrinsic free space impedance (120π). The wave impedance of the near field is calculated based on the effective constitutive parameters as

$$Z = \sqrt{\frac{\mu_{\text{eff}}}{\epsilon_{\text{eff}}}}\ [\Omega], \tag{3.46}$$

and in case this is something other than the intrinsic free space impedance, there will be added losses.

As an example, it was shown that the effective angular divergence frequency (ω_d) for a square array of split ring cylinders, can be calculated from its physical dimensions (Pendry et al., 1999). The variable d is the distance between the split rings and r is the radius of the outer ring, where

$$\omega_d = \sqrt{\frac{3dc_0^2}{\pi^2 r^3}} \ [\text{rad s}^{-1}], \tag{3.47}$$

where ω_d equals $2\pi f_d$.

Calculating the constitutive parameters of a unit cell

The effective permeability of a unit cell can unfortunately not be exported directly from COMSOL Multiphysics as an intrinsic material property. Instead, it has to be calculated based on its simulated impedance response. Balanis shows how the electric and magnetic dipole moment is utilized to find the constitutive parameters (Balanis, 2012).

Permeability The average magnetic dipole moment per unit volume (M) is found from the number of current loops (N_m), area (s) per loop and the induced magnetization current (I_m) (Balanis, 2012), which is denoted as

$$M = \hat{n} N_m (I_m s) \ [\text{A m}^{-1}]. \tag{3.48}$$

The magnetization current is the current that is induced on the resonator when it is positioned within the near-field of an antenna. The induced current flows along the conducting boundaries of the resonator. COMSOL Multiphysics takes the thickness of the conductor into account and projects this current onto the boundary surface area (S_0) as a surface current density. The magnetization current (I_m) can therefore be calculated by multiplying the extracted surface current density per meter with the width of the conductor (dy). This width is perpendicular to the propagating direction of the current.

Alternatively, it can be calculated directly from the current density per volume as

$$I_m = \iint_{S_0} J_m \cdot d\text{s} \ [\text{A}]. \tag{3.49}$$

The total magnetization current contains contributions from all three directions, which have to be calculated separately and summarized. The various dimensions and areas are visualized in Figure 3.6.

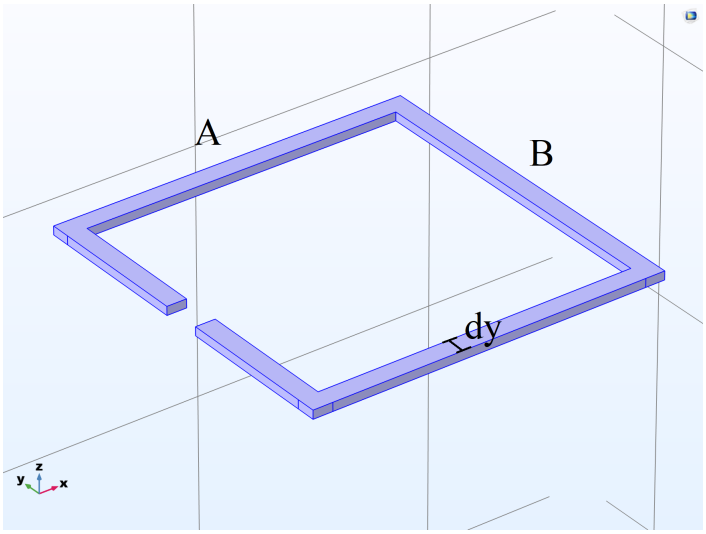

Figure 3.6: Unit cell properties; (a) The area (s) of the current loop is the length A multiplied with B, (b) boundary surface area (S_0) is marked with blue colour and (c) dy represents the width of the conductor, which is multiplied with the surface current in the propagating direction to find the current

The magnetization is the product of the magnetic susceptibility (χ_m) and the magnetic field intensity (H), as

$$M = \chi_m H \ [\mathrm{A\,m^{-1}}]. \tag{3.50}$$

The permeability is expressed with the help of the absolute permeability and the magnetic susceptibility as

$$\mu = \mu_0(1 + \chi_m) \ [\mathrm{H\,m^{-1}}]. \tag{3.51}$$

Permittivity The electric polarization is found from the current loops per unit volume (N_e), the charge (Q) and the length of the resonator (l_{average}) in the direction of the electric field (Balanis, 2012), where

$$P = N_e Q l_{\text{average}} \ [\mathrm{C\,m^{-2}}]. \tag{3.52}$$

The electric polarization vector (P) is related to the electric field intensity (E), by the electric susceptibility (χ_e), where

$$P = \epsilon_0 \chi_e E \ [\mathrm{A\,m^{-1}}]. \tag{3.53}$$

The permittivity is expressed with the help of the absolute permittivity and the electric susceptibility, as

$$\epsilon = \epsilon_0(1 + \chi_e) \ [\mathrm{F\,m^{-1}}]. \tag{3.54}$$

With these equations, it should be possible to calculate the constitutive parameters, based on the extracted surface currents on the unit cells and the field intensities. The equations imply that the positioning of the gap on the unit cell, should not have any major impact on their performance.

3.7 Possible application for antennas with reduced resonance frequency

The focus of this thesis is to develop an understanding of the potential of material-based miniaturization with magneto-dielectrics. However, the value of material-based miniaturization can only be determined by how useful it is for solving practical use cases.

Some possible applications for small microstrip antennas with reduced resonant frequency has been identified through the work with this thesis;

- AIS (Automatic Identification System) antennas which can be placed on board satellites and on small ships
- DVB-T (Digital Video Broadcast-Terrestrial) antennas for hand-held devices
- Antennas for mobile broadband routers
- Tactical low-profile antennas for UHF, VHF and HF (High Frequency) -range for mounting at vehicles and man packs, or camouflaged in the environment

Chapter 4

Design and analysis of a reference microstrip antenna

To provide a baseline for the reduction of resonant frequency, this chapter will include the design of a reference microstrip antenna. This antenna will be designed with an air-filled substrate and a probe-fed square patch, where the latter will be reused in the later designs with other substrates.

4.1 Geometry

The geometry of the reference antenna is chosen with inspiration from the Cubesat standard, which has maximum dimensions of 10x10x10 cm^3, which also is practical in terms of Additive manufacturing. Additive manufacturing refers to technologies which build physical objects one layer a time and is commonly called ”3D printing”. The design includes a ground plane of 10x10 cm^2 and a radiating patch with a ”random” width of 7.1 cm. The height should ideally be the difference between the patch and ground, divided by six, according to Equations 3.23 and 3.24. Calculations of the feed depth are performed in Appendix B, based on Equations 3.30 to 3.33.

The reference antenna was given the following dimensions;

- Square patch, which is 7.1 cm wide and has a 7.1 cm length
- Height of 4.8 mm
- Ground plane of 10x10 cm^2
- Feed depth of 2.28 cm

The reference antenna was modelled in COMSOL Multiphysics as shown in Figure 4.1, and the antenna parameters are extracted to provide a reference for the future reduction of the resonant frequency.

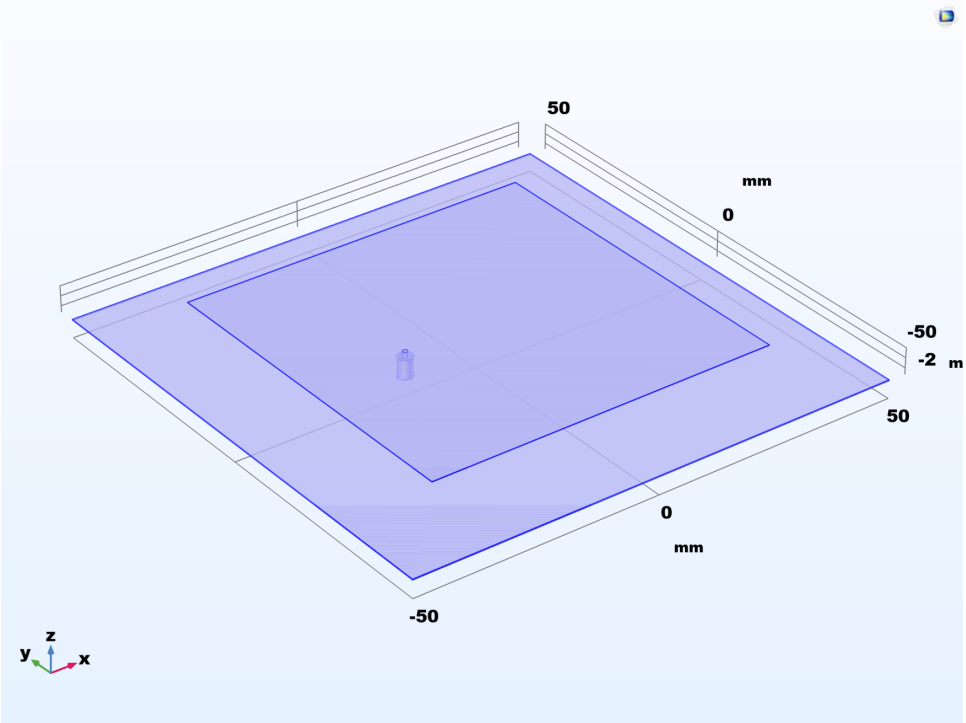

Figure 4.1: Reference antenna geometry

4.2 Analysis

4.2.1 Resonance and bandwidth

A half-wavelength patch of 7.1 cm should resonate at 2.112 GHz, according to Equation 3.19. This is the case for zero height and length extensions from fringing fields should not be taken into consideration.

For a square microstrip of similar patch dimensions, where the height now is increased to 4.8 mm, the fringing fields result in an increased electrical length. This added length reduces the resonance numerically to 1.93 GHz and is simulated to 1.875 GHz, as seen in Figure 4.2 with a 3.2% -10 dB impedance bandwidth.

This added height where the patch is now physically short relative to the resonance frequency, has made the antenna slightly capacitive in accordance with Equation 3.25.

4.2.2 The movement of electric and magnetic fields within the substrate

Later positioning of future anisotropic substrates must be in accordance with how the electric and magnetic field intensities move within the substrate at resonance. With this in mind, a plot of the electric field intensity at resonance was created, which is illustrated in Figure 4.3. This plot concludes that the electric field intensity is strong under the radiating edges of the patch.

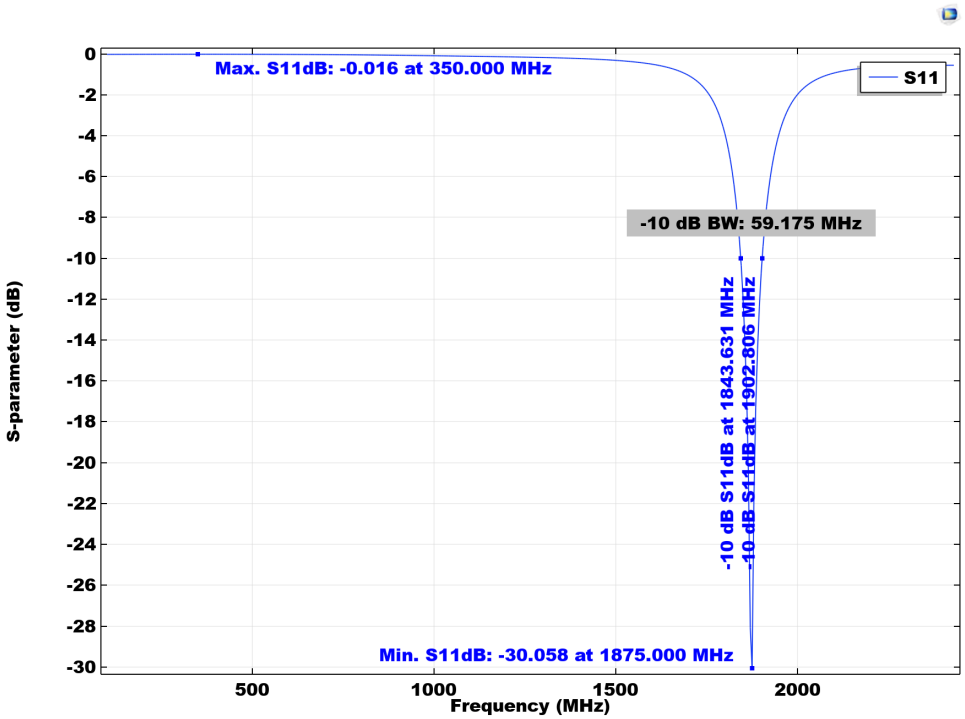

Figure 4.2: Reference antenna simulated of S_{11}

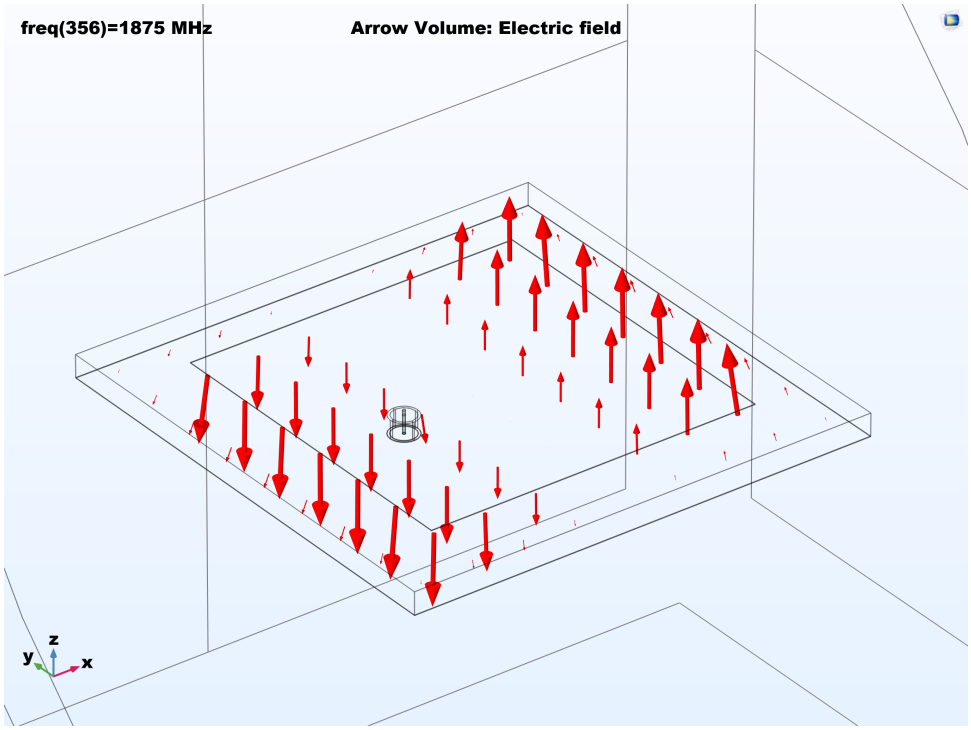

Figure 4.3: Electric field intensity between patch and ground

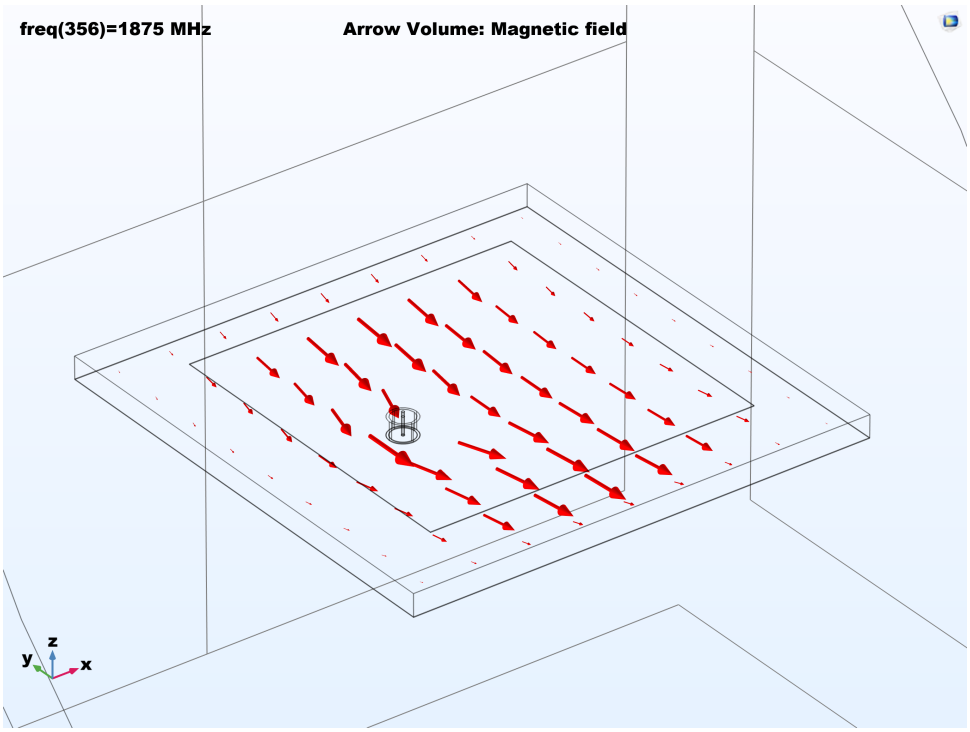

Figure 4.4: Magnetic field intensity between patch and ground

Similarly, a plot of the magnetic field intensity shows that it is resonating between the non-radiating edges of the patch and is weak close to the radiating edges. This is illustrated in Figure 4.4. The magnetic field intensity seems to be strong in the middle of the substrate, where the electric field intensity is weak.

4.2.3 Loss

The radiation efficiency was 97.3% for the probe-fed reference antenna, where the loss of 2.7% is expected to be due to the remaining impedance matching of the feed and resistive losses in the conductors.

4.2.4 Far-field gain

Patch antennas are known for their relatively high directivity, which is confirmed with a plot of the realized far-field gain. The simulations show a maximum gain of 9.0 dBi and an 8.9 dBi directivity. This is illustrated in Figure 4.5.

4.3 Summary

The COMSOL Multiphysics simulations confirm Equation 3.19 to 3.33, and the reference antenna provides a high gain and low loss.

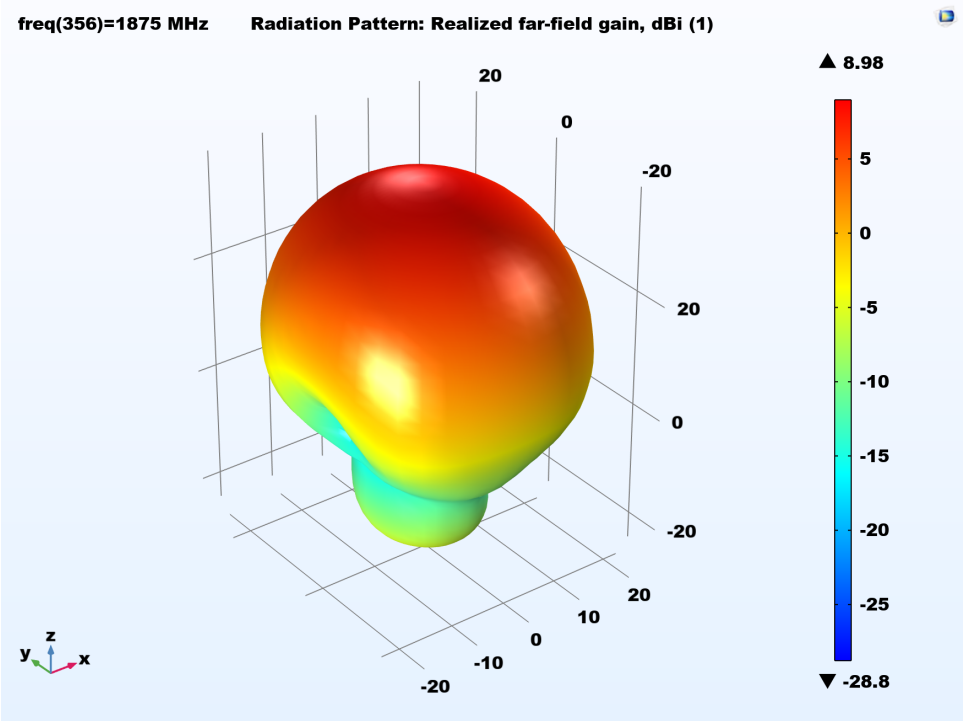

Figure 4.5: Reference antenna simulated realized far-field gain

The reference antenna provided the following simulated antenna parameters;

- Resonance at 1.875 GHz, due to length extended resonance at 2.112 GHz
- -10dB impedance bandwidth of 3.2%
- Directivity of 8.9 dBi
- Loss of 2.7%

Chapter 5

Design and analysis of antenna with natural magneto-dielectrics to reduce resonant frequency

This chapter presents the design and analysis of a microstrip antenna with a natural magneto-dielectric substrate, to reduce the resonant frequency.

5.1 Choice of magneto-dielectric substrate

It exists a plethora of substrates which can be utilized in microstrip antennas. The main purpose of the substrate is to distance the patch from the ground, and many of these substrates have dielectric properties. Magnetic substrate are more rare since they add a magnetic loss component. However, some magnetic substrates are developed for research and some have been made commercially available. One such substrate is made available by Roger Corporation and is named MagTrex 555 (Rogers Corporation, 2019b). The identified substrates are presented in Table 5.1 and sorted based on their real relative permeabilities. Sintering ferrites would far exceed the scope of this thesis, and ordering tailored materials would require financial resources, which were not available. MagTrex 555 (Rogers Corporation, 2019b) was chosen to be utilized, due to its commercial availability. The MagTrex 555 has an almost matched permittivity and permeability

Table 5.1: Magneto-dielectric materials with their relative permittivity and permeability exemplified for 200 MHz (DVB-T)

Materials	μ_r	$\tan\delta\mu$	ϵ_r	$\tan\delta\epsilon$	Reference
MagTrex 555	5.9	0.026	6.5	0.019	(Rogers Corporation, 2019b)
Ba3Co2Fe24O41	6.91	0.01	6.88	NA	(Bae et al., 2009)
Ba(CoTi)1.22Fe9.56O19	18.3	0.034	18.1	0.0028	(Li et al., 2019)
Ba3Co1.6Mn0.4Fe24O41	20	0.01	20	0.014	(Kim et al., 2014)

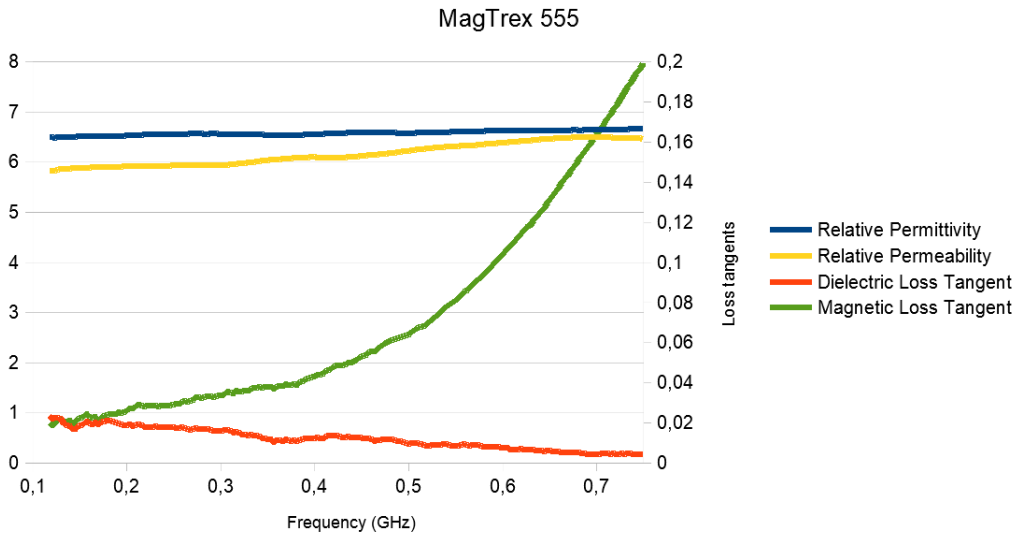

Figure 5.1: MagTrex 555 constitutive parameters

around six and low loss-tangents. It comes as a panel with an area of 305 x 457 mm^2. It could be delivered either electro-deposited with 35 µm copper foil or as unclad. The available panels have a thickness of either 1.02, 2.54, 6.60, 1.52, 3.56, 2.03 or 5.08 mm. A table with the constitutive parameters was sent from Rogers Corporation together with MagTrex 555 (Rogers Corporation, 2019b) and they are presented in Figure 5.1.

5.2 Geometry

To simulate the microstrip antenna with MagTrex 555 as a substrate, the reference antenna required some adjustments to the design. The width and length of the patch were kept identical as for the reference antenna, but the height had to be increased to encompass the substrate. The substrate which was purchased from Rogers Corporation, came electro-deposited with copper, had a height of 2.54 mm and an area of 305x457 mm^2. Appendix B contains calculations of the new feed depth and Equation 3.41 claims the loss to be proportional to the width of the substrate. To understand better the implication of substrate dimensions on the antenna parameters, Table 5.2 was created with a small range of realistic dimensions and their resulting effect on efficiency and bandwidth. The parameters were extracted with a 5 MHz accuracy plot.

5.2.1 Reduction of resonance frequency

Table 5.2 claims that all heights with a 10 cm wide substrate, result in resonance at 370 MHz, which is a reduction of resonant frequency by 82.5%. At 370 MHz the refractive index of MagTrex 555 is, according to Figure 5.1, around 6.2. If this is the effective refractive index of the

Table 5.2: Substrate dimension and the following antenna parameters at reduced resonance frequency with 10x10 cm^2 ground plane, including the -10 dB impedance bandwidth

Width	Height	Frequency after reduction	Bandwidth	Efficiency
100mm	7.62 mm	370 MHz / 82.5%	3.9%	20.1%
100mm	10.16mm	370 MHz / 82.5%	4.0%	23.9%
71 mm	10.16 mm	500 MHz / 76.3%	3.3%	39.3%
100 mm	12.7 mm	370 MHz / 82.5%	4.1%	28.5%
71 mm	12.7 mm	500 MHz / 76.3%	2.4%	46.2%
100 mm	25 mm	370 MHz / 82.5%	4.4%	33.0%

antenna, it should offer a resonant frequency of around (1/6.2), which is what, that is simulated. These simulations thereby imply that the absolute permeability and permittivity of the substrate also is the effective permeability and permittivity of the near field of the antenna. This for the case where the width and length of the substrate are kept constant at 100 mm. However, according to a video from Rogers Corporation (Rogers Corporation, 2019a), this should only be valid for the permittivity, while the effective permeability should be a volume fraction of the substrate dimension relative to the near-field sphere of the antenna. During the scope of the thesis, it was not found any equations to calculate the effective permeability and this lack of suitable equations has been confirmed by other studies (Niamien et al., 2011).

A large height itself is expected to reduce the resonant frequency, due to length extensions, according to Equation 3.22, but this is not visible in Table 5.2.

5.2.2 Radiation efficiency

Equation 3.41 claims the radiation efficiency to improve with a less wide substrate. Simulations in Table 5.2 shows this to be true, however, this reduction of substrate volume does also reduce the bandwidth as claimed by Equation 3.44 and leads to a higher resonance frequency.

5.2.3 Far-field gain

The directivities of the simulations in Table 5.2 are very close to that of an ideal omnidirectional dipole antenna, which has a directivity of 2.2 dBi. These simulations have been made with a ground plane which has dimensions that are close to the radiating patch. A larger directivity could be achieved if the ground plane was enlarged to half a wavelength, as seen in Figure 5.4.

5.2.4 Dimensions

The 10.16 cm height was chosen for further studies since an excess height would result in a higher need for impedance matching. Feed depth

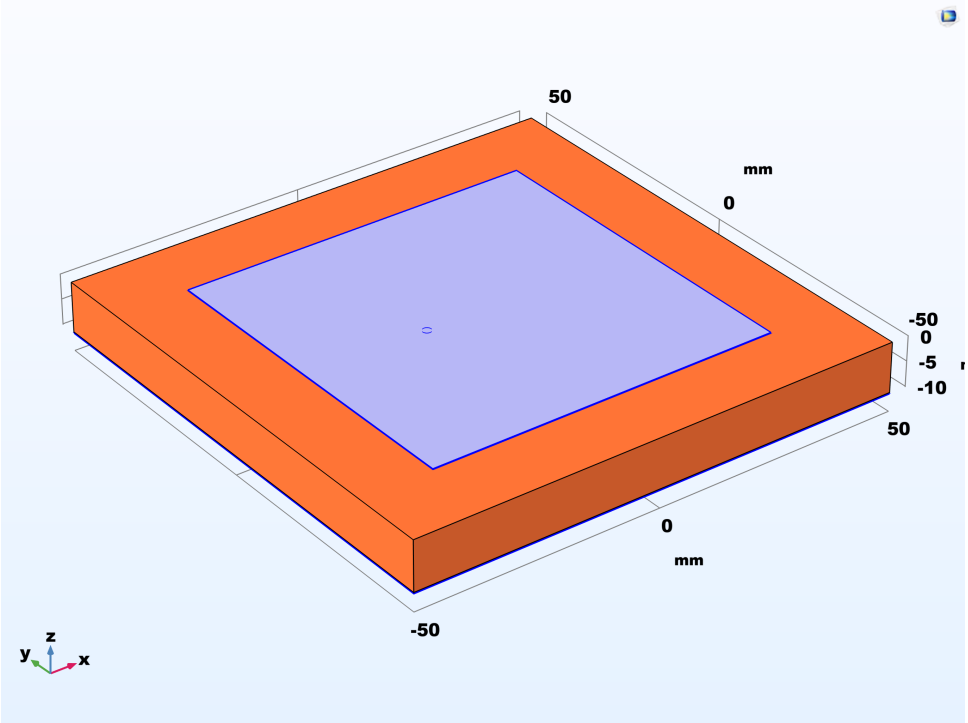

Figure 5.2: Magneto-dielectric geometry, where orange illustrates MagTrex 555 and a small ground plane under

was first calculated in Appendix B, according to Equations 3.30 to 3.33. Magnetic materials should according to Equation 3.26, alter the impedance of the antenna. A Smith plot showed that the calculated feed depth was not ideal, and the feed depth was reduced to 2.4 cm from the radiating edge of the patch.

Geometry for the magneto-dielectric antenna was set to the following dimensions, based on the calculations in Appendix B;

- Square patch, which is 7.1 cm wide and has a 7.1 cm length
- Height of 10.16 mm
- Ground plane of 40x40 cm^2 to maximize directivity
- Probe fed
- Feed depth of 3 cm but tuned down to 2.4 cm

5.3 Analysis

The antenna response was simulated in COMSOL Multiphysics, which allowed the extraction of antenna parameters. The simulations were made with a probe feed.

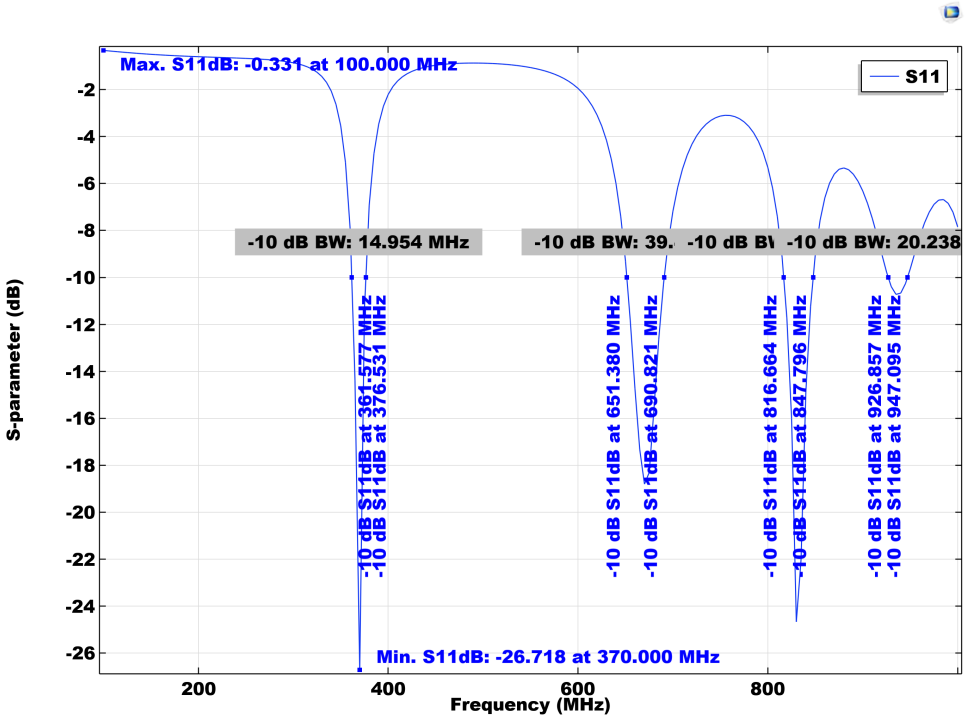

Figure 5.3: Magneto-dielectric antenna simulated S_{11}

5.3.1 S_{11} plot and bandwidth

The S_{11} plot shows multiple resonances, as seen in Figure 5.3. Since the magnetic loss tangent is increasing with frequency; the lowest resonance which is 370 MHz, was chosen for further analysis.

5.3.2 Radiation efficiency

The simulated radiation efficiency was 23.9%. The losses are according to COMSOL, due to the electromagnetic losses in the substrate.

5.3.3 Far-field gain

Due to high magnetic losses, the maximum realized gain was only -6.7 dBi when the ground covered the area of the substrate, as seen in Figure 5.4. This is with a small ground plane, which limited the maximum directivity to 2.2 dBi. When the ground plane was enlarged to half a wavelength, the maximum realized gain improved to 0.8 dBi based on a new maximum directivity of 6.3 dBi. An additional effect of increasing the ground dimensions is that the -10 dB impedance bandwidth was reduced to 3.9% and the resonance frequency increased by 6.7%, which is a slightly smaller reduction of the resonance frequency.

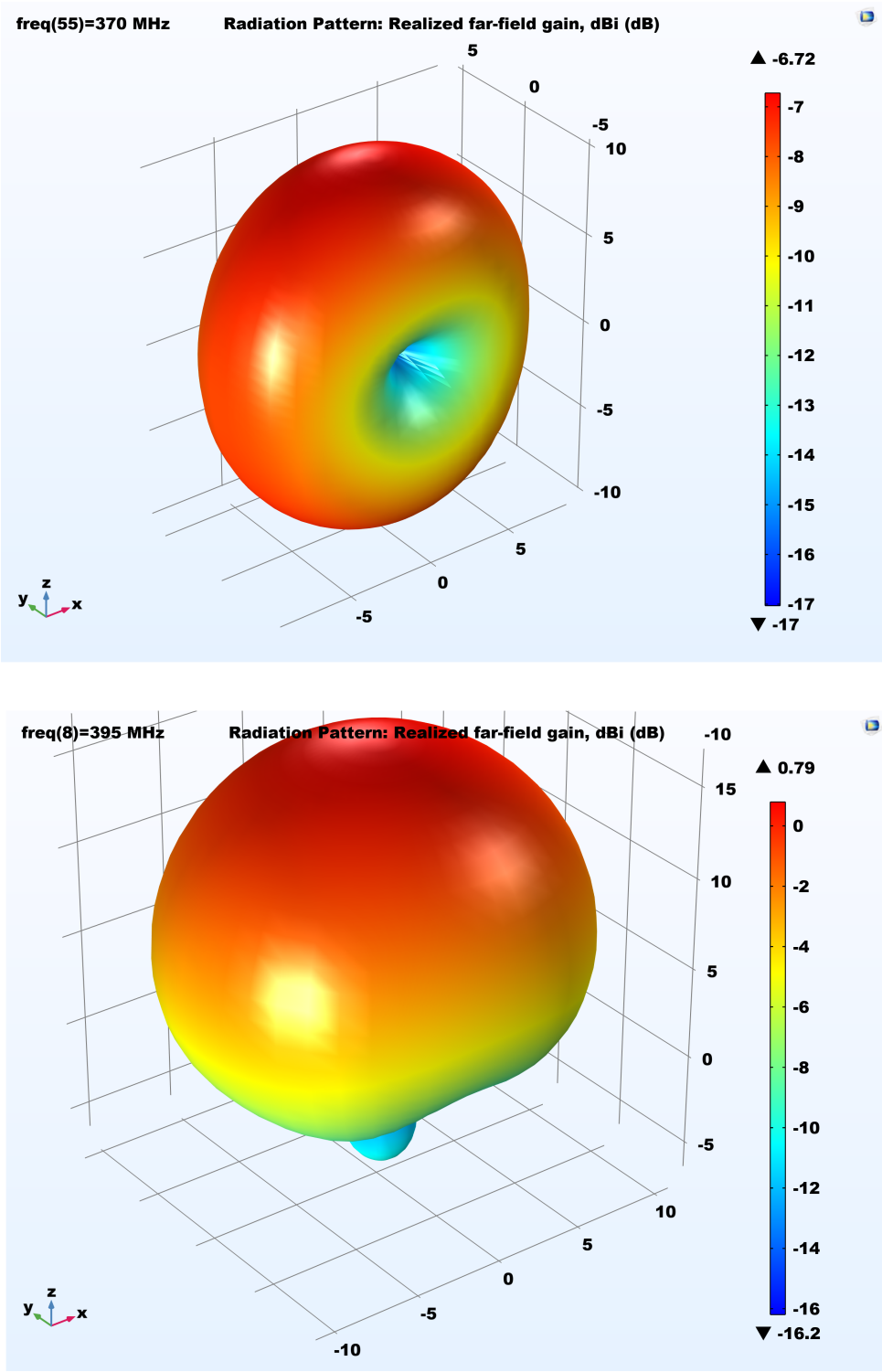

Figure 5.4: Magneto-dielectric antenna simulated realized far-field gain where the upper figure is with a small ground at 10x10 cm^2, and the lower figure with a large ground at 40x40 cm^2 and a slightly higher resonance frequency

The following antenna parameters were recorded from the simulation of a magneto-dielectric antenna with a substrate which had a volume of 10x10x1.0 cm^3, and ground of half a wavelength;

- Resonance at 370 MHz, if μ_{eff} equals μ
- 82.5% reduction of resonance frequency
- -10 dB impedance bandwidth of 4.0%
- Directivity of 6.3 dBi when the ground is set to half a wavelength
- Radiation efficiency of 23.9%

5.4 Manufacturing with etching

MagTrex 555 is a commercial product which is produced by Roger Corporation. Upon arrival, it was cut into 10x10 cm^2 pieces. The product came electro-deposited with copper, which required an etchant solution to remove the excess material. Sodium persulfate was ordered as a powder and had to be dissolved in distilled water, and the powder had a solubility of 55.6 g per 100 ml at room temperature. Due to the thickness of the electro-deposited layer of copper on the substrate, the acid was quickly saturated and had to be changed often. The setup is photographed in Figure 5.5.

Figure 5.5: Etching with sodium persulfate

After the etchant solution had removed the surplus copper, an antenna was put together with a connector, coaxial cable, and a ground plane cut

from a 0.5 mm thick aluminium sheet. The antenna is illustrated in Figure 5.8.

5.5 Measurements

The S_{11} scattering parameter was measured for the prototype antenna, with varying substrate thickness. The feed between the ground and the patch was not shielded during the test. Based on immediate measurements and that the calculations did not include the magnetic permeability, the feed depth was reduced to approximately 1 cm. However, the impedance matching was still low with the probe feed, and the antenna was modified to a coupled feed, as suggested during measurements in the next chapter. This helped significantly to achieve impedance matching.

Resonance frequency and bandwidth

To grasp a practical understanding of how the substrate and patch dimension together affects the resonance frequency, a square microstrip antenna was initially constructed with a square patch that had a 10 cm width and a 10.2 mm height. The antenna showed two resonances, one weak resonance at 476 MHz, and one stronger resonance at 709 MHz where this had a -10 dB impedance bandwidth measured to 4.4%. The patch width was then reduced to 7.1 cm, which made no difference in the resonance frequency. The patch length was set to 7.1 cm as simulated, which changed the resonances to 495 MHz and 748 MHz and can be seen in Figure 5.6. This proves the resonance to be highly dependent on the length of the patch, as expected according to Equation 3.19. The lowest resonance frequency at 495 MHz, is a 76.6% reduction from 2.112 GHz.

The antenna was then measured multiple times, with varying substrate heights, which showed that the resonance frequencies were highly dependent on the height. Rogers Corporation claimed that the resonance frequency would be reduced when the height of the substrate is increased. This is because the effective permeability increases when the volume of the substrate fills a larger portion of the near field (Rogers Corporation, 2019a). Contrary to the simulations with COMSOL Multiphysics [1], the lower resonance of 370 MHz was not identified during measurement, which supports the suspicion that COMSOL Multiphysics with the current defined models, did not sufficiently find the effective constitutive parameters of the near field.

Radiation efficiency

The anechoic chamber at the University is not built for frequencies below 1 GHz and the simulations of directivity claim an omnidirectional radiation pattern with a small ground. It was decided to utilize Wheeler's cap method to measure radiation efficiency, as described in Equation 5.7. A

[1] http://comsol.com

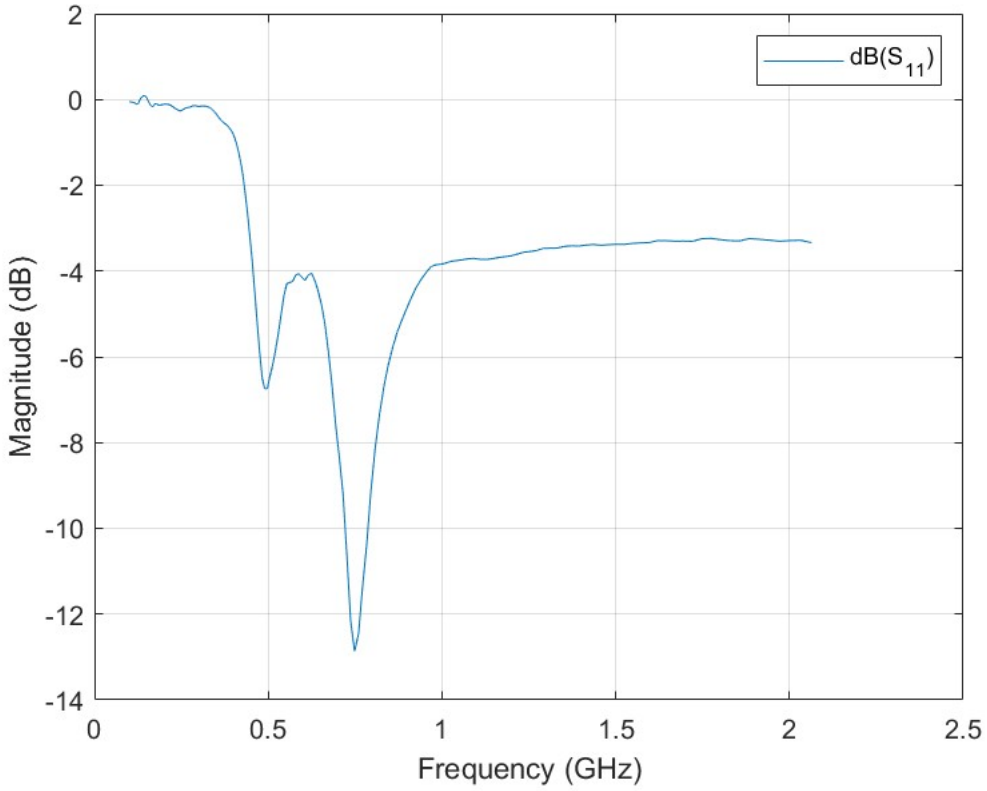

Figure 5.6: Measured magneto-dielectric antenna S_{11}. It has a 10.2 mm height and a 7.1 mm width and length

Figure 5.7: Wheeler's cap was constructed with aluminium foil, copper tape and cardboard

Wheeler's cap was built with cardboard, aluminium foil and copper tape to close all gaps. The cardboard had a width and height, which was large enough but it was challenging to position the antenna perfectly in the middle. The copper tape did not include conducting glue, and the aluminium foil was not able to close the entrance completely. This may enlarge the error margin since it allows radiation to leave the cap. The final radiation efficiency should therefore be higher than the experimental value.

It seemed easier to achieve perfect impedance matching with a low height, and the antenna height was therefore reduced to 7.62 mm before it was tested with Wheeler's cap. The antenna measured an S_{11} reflection of -22.4 dB in free space and with Wheeler's cap of -10.66 dB MHz. This gives a radiation efficiency of 14%. A simulation with the loss tangents from Figure 5.1 at 620 MHz, resulted in a radiation efficiency of 10%, which confirms the high losses during measurement.

Weight

The weight of a single magneto-dielectric substrate is 85 g for a square panel which is 10 mm wide, which equals approximately three $\mathrm{g\,cm^{-3}}$. A need for multiple panels with substrate results in a large weight, which again makes it less suitable for space, air-born and handheld devices.

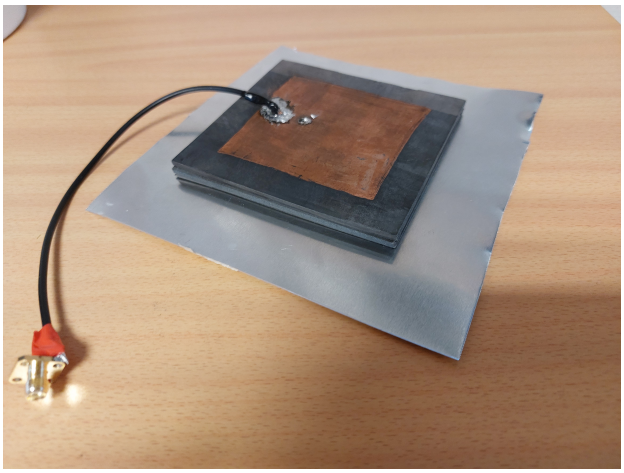

Figure 5.8: A probe-fed prototype with MagTrex 555 was constructed for measurements with slightly enlarged ground

5.6 Summary

The measured reduction of resonance frequency with MagTrex 555 was around 76.6% and highly dependent on the substrate thickness. There is considerable losses, due to the large magnetic loss tangents. However, the magnetic properties had a favourable effect on the -10 dB impedance bandwidth, which was measured to 4.4%. With a ground plane of half a wavelength or more, the directivity should be comparable to the directivity of the reference microstrip antenna.

Chapter 6

Design and analysis of antenna with metamaterial to reduce resonant frequency

This chapter presents the design, manufacturing and measurement of a microstrip antenna which includes unit cell resonators. The purpose is to understand how it performs relative to the microstrip antenna with MagTrex 555. The design of the metamaterial antenna is based on a similar approach which was confirmed with measurements (Kärkkäinen and Ikonen, 2005).

6.1 Unit cell design

There are multiple possible unit-cell designs, as seen in Figure 3.4, but C-ring resonator was chosen since it offered a very simple design. To achieve a wide bandwidth; the antenna must operate below the divergence frequency, in the spectral range where there is a weak dispersion material characteristic, low loss-behaviour, and an acceptable high impedance resulting from an acceptable high permeability (Ikonen et al., 2006). The numerical calculated resonating frequency for a 7.1 cm microstrip without added impedance due to fringe fields is 2.112 GHz, and the unit cell was designed in COMSOL Multiphysics [1] according to the suggested dimensions in Figure 3.4. The unit cell will together with the length extension, both contribute to a reduction of the resonant frequency.

Figure 4.4 illustrates that the magnetic field resonates between the non-radiating edges and are strongest under the centre of the radiating patch. The unit cells will therefore be positioned vertically between the ground and the radiating patch, as illustrated in option (c) in Figure 3.3.

In COMSOL Multiphysics, a box was drafted to encapsulate the unit cell, with two opposite walls in the x-direction defined as PMC (Perfect Magnetic Conductor), two walls in the y-direction defined as PEC (Perfect Electric Conductor) and the top in the z-direction as a port. The perfect

[1] http://comsol.com

conductors set the corresponding tangential components to zero. The actual resonator is seen in Figure 3.6.

Contrary to the suggested dimensions for the resonators in Figure 3.4, simulations demanded a larger diameter of the resonator, to achieve divergence at the requested frequency. The simulations proved the length of unwrapped resonators to be close to a half wavelength. The C-ring resonator required a 14.5 mm diameter to achieve the requested divergence, while a square spiral resonator required a diameter of 10 mm.

The single C-ring resonator dimensions were set to the following dimensions;

- Diameter = 14.5 [mm] (Length of A in Figure 3.6)
- Gap = 3 [mm] (Gap in B in Figure 3.6)
- Conductor width = 0.8 [mm] (Width of dy in Figure 3.6)

A strong resonance was achieved when the volume was reduced to around 3.7 cm^3, which sets the favourable distance between unit cells.

COMSOL does not extract the induced constitutive parameters, but it allows the extraction of the surface current over the boundaries of the unit cells, and with this, it was possible with Equations 3.48 to 3.54, to then calculate the magnetization and electric polarization. These calculations are utilized to plot both the permeability and permittivity at each frequency step, which can be seen in Figure 6.1. Since the resonators later during manufacturing will be painted onto a sheet, and the current will move around the resonator; it is only necessary to find the surface current density in the y-direction, to find the total current.

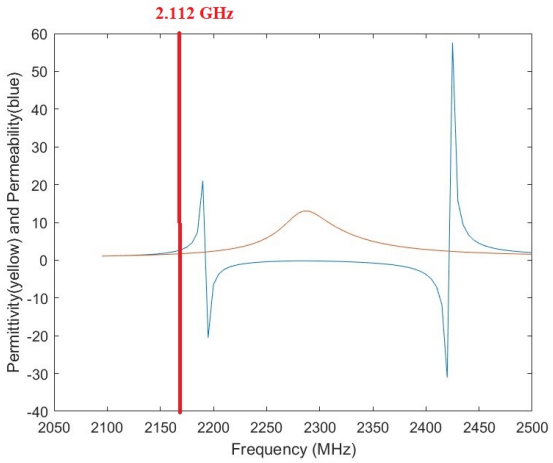

Figure 6.1: Plotted relative permeability (blue) and permittivity (yellow) of the unit cell simulation in the range 2.1 GHz to 2.5 GHz

At 2.112 GHz, the relative magnetic permeability was calculated to 2.79 and the relative electric permittivity to 1.12. The constitutive parameters are unmatched, which results in reduced radiation efficiency due to

remaining matching to the far-field impedance. Together they provide a refractive index of 1.76, which could offer a 57% reduction of the reference antenna resonance if the cells are stacked perfectly in an infinite array.

6.2 Geometry

The height of the microstrip antenna was increased to 33 mm, and the design is illustrated in Figure 6.2.

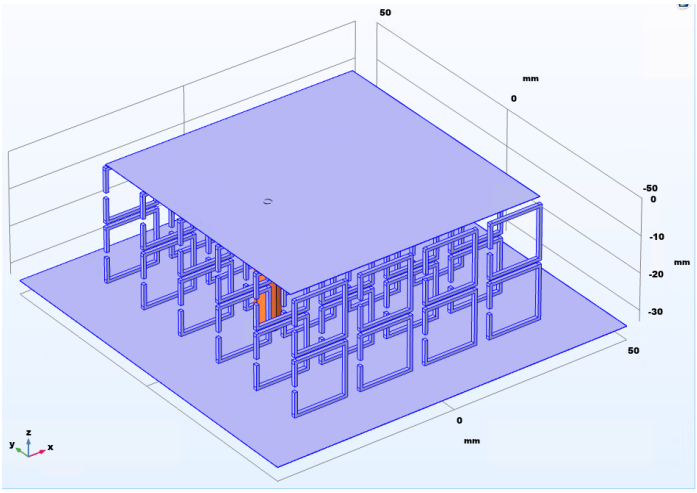

Figure 6.2: Metamaterial antenna geometry with resonators

The electromagnetic response from a single unit cell is useful, but it is the total array of unit cells which will determine the effect on the microstrip antenna.

Table 6.1: Number of cells, the distance between them and the following antenna parameters at the reduced resonance frequency, including the -10 dB impedance bandwidth.

Cells	Distance	Frequency after reduction	Bandwidth
48	29	1180 MHz / 44%	8.6%
48	14.5	1040 MHz / 51%	7.5%
104	14.5	1060 MHz /50%	8.5%

Table 6.1 shows that the number of resonators and the distance between them affect both the resonance frequency and the -10 dB impedance bandwidth. Similar to the magneto-dielectric antenna, a large substrate area of unit cells, is necessary to ensure a wide bandwidth. A larger number of unit cells within this area may reduce the resonance frequency even further.

For simplicity, 48 unit cells with 29 mm between them were chosen for prototyping. The realized volume was increased to 4.9 cm^3 since it seemed practical during the later for manufacturing.

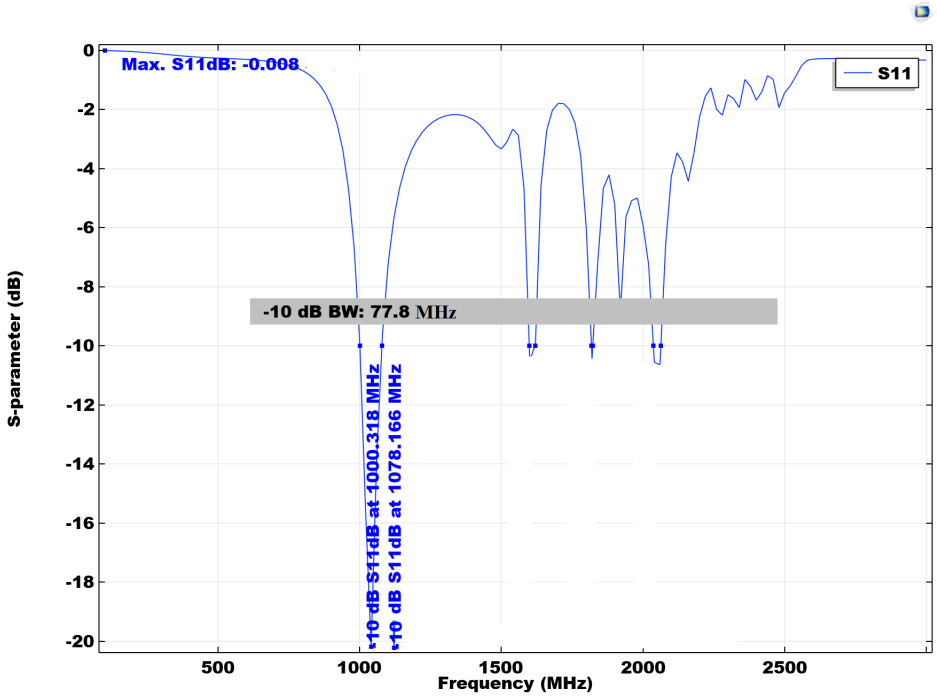

Figure 6.3: Metamaterial antenna simulated S_{11} with resonance at 1.04 GHz

6.3 Analysis

To understand if the microstructures functions according to the intention, COMSOL Multiphysics was again utilized to extract the antenna parameters.

6.3.1 S_{11} plot and bandwidth

The S_{11} plot for the second option in Table 6.1 is seen in Figure 6.3. The simulated antenna, with 48 unit cells and 14.5 cm between the sheets, had a resonance at 1.04 GHz and a -10 dB impedance bandwidth at 7.5%. This is a reduction of resonance frequency by 51% relative to the numerical resonance frequency of a patch with similar dimensions.

6.3.2 Radiation efficiency

The simulated radiation efficiency was 95.1% due to both any feed mismatch and resistivity in the conductors. This seems very optimistic, since other studies (Ouedraogo et al., 2012) suggest a much lower radiation efficiency as a result of reduced antenna volume, as explained by Equation 3.16.

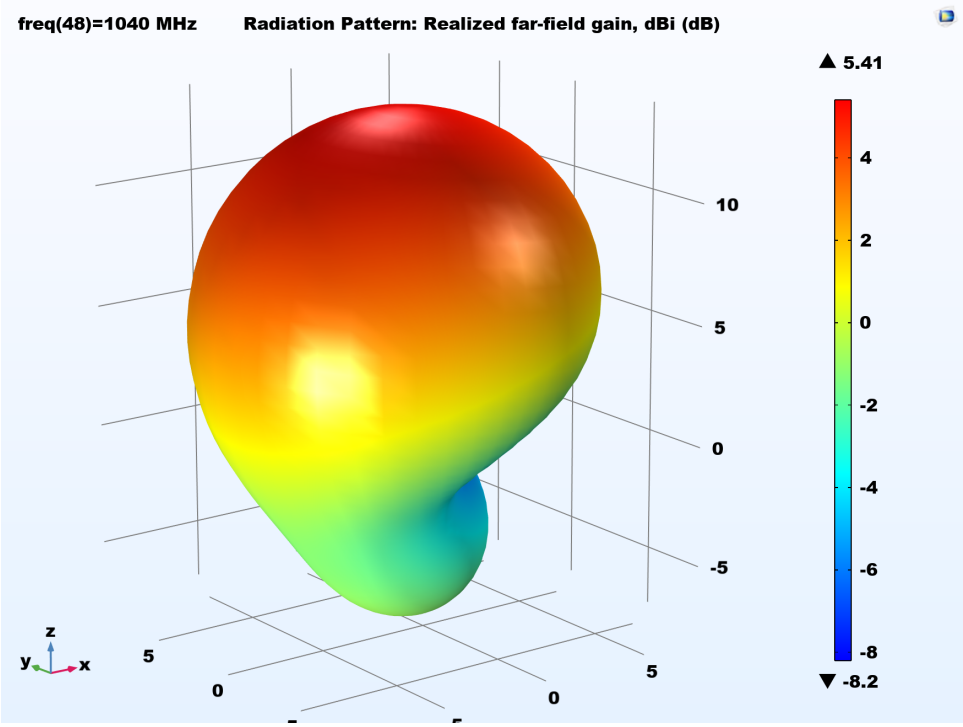

Figure 6.4: Metamaterial antenna simulated realized far-field gain

6.3.3 Far-field gain

The antenna reached a simulated maximum directivity of 5.4 dBi, and with the mentioned low losses, the maximum simulated realized gain was also 5.4 dBi. The simulated realized gain can be seen in Figure 6.4.

The square patch probe-fed antenna with resonators had the following simulated properties;

- Feed depth of 2 cm, reduced from the calculated 2.8 cm
- Square patch, which is 7.1 cm wide and has a 7.1 cm length
- Ground plane of 10x10 cm^2
- Resonance at 1.04 GHz
- Reduction of resonance frequency by 51%
- -10 dB impedance bandwidth of 7.5%
- Directivity of 5.4 dBi

6.4 Additive manufacturing

The antenna was modelled in Solid Works and then exported as STL files. The files were then imported into Lychee Slicer [2] to add supporting structure and slice the model into printer-compatible layers. The designs

[2] https://mango3d.io/

were printed through stereolithography (SLA) on an Anycubic mono X [3], which has a resolution of 50 µm. SLA utilizes an ultraviolet (UV) laser to cure liquid photopolymer resin into a solid, and one available resin was the Prima value UV resin [4], which was utilized to realize the three-dimensional models. To achieve suitable rigidity in the structure, 1 mm was used as a minimum dimension. After the models were manufactured, they were cleaned with isopropanol and cured with additional ultraviolet radiation. The support structure was then removed by hand, and any uneven edges were sanded down.

The design consisted of two parts; an antenna frame which separates the ground from the patch, and then sheets with unit cells, which all are seen in Figure 6.5. The sheets could be slid into the antenna frame vertically between the ground and the radiating patch. The datasheet for the resins, which was available did not specify the dielectric properties of the materials. The vendors were contacted, but they were not able to provide this information. The resins which were available for SLA are not expected to have any magnetic properties, but the relative permittivity was set to an approximate value of 3.5 (Veselý et al., 2018). The SLA printer and its configuration are also expected to affect the final dielectric properties. A more accurate approach would be to choose a resin made for RF -communication which specifies the frequency-dependent permittivity in a datasheet and then confirms these properties with material-specific measurements. To limit the scope of work and cost, the structure was produced with as little resin as possible, which reduces the error margin. The later simulations were performed with both a dielectric resin and a resin without dielectric properties. Simulations show that around 10% of the reduction of resonance frequency at this frequency was due to the dielectric properties of the resin. The dielectric properties are expected to narrow the bandwidth simultaneously as it may contribute to impedance matching of the resonators.

6.4.1 Antenna frame

The purpose of the antenna frame was to hold the ground, patch, feed and resonators together. It was considered to utilize a conductive paint for the radiating patch and the ground. This would have resulted in a very low weight, but it was not practical for soldering a feed. A test with conductive glue proved the glue to be highly resistive in the UHF range. For prototyping, it proved more flexible to cut 0.5 mm sheet metals and connect wire to them. Soldering an SMA (SubMiniature version A) connector onto the sheet metal was challenging, and the connector was instead screwed in place.

[3] https://www.anycubic.com/
[4] https://www.3dprima.com/

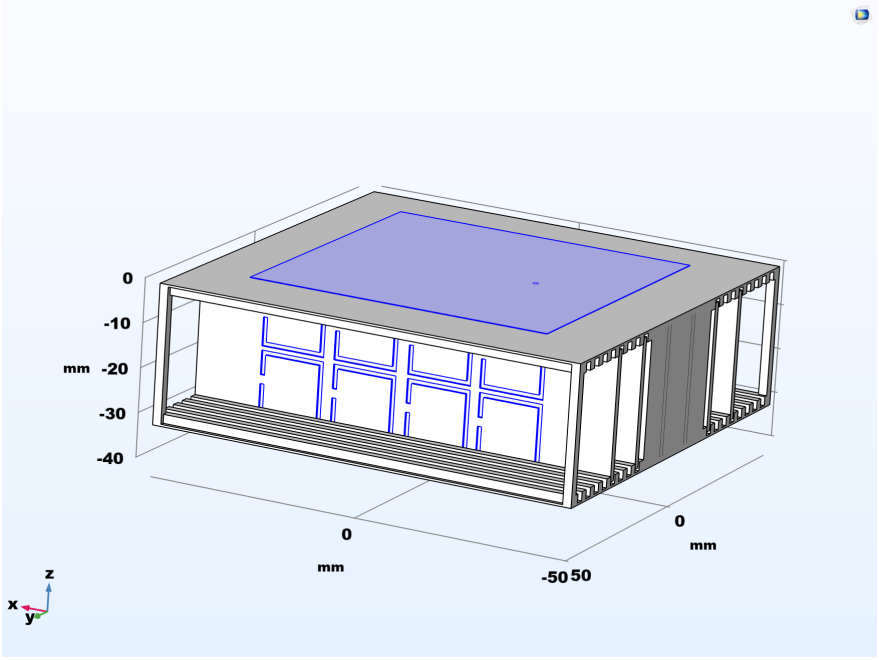

Figure 6.5: Metamaterial antenna with resonator sheets

6.4.2 Unit cell conductor

To manufacture the unit cells, a conductive spray was utilized. One alternative was produced by MG Chemicals [5] and named Super Shield silver-coated copper conductive coating aerosol 843AR-340G (MG Chemicals, 2022). It is a highly conductive acrylic paint which is designed to reduce electromagnetic and radio frequency interference. The minimum thickness of conductive paint is determined by the skin depth at the intended resonating frequency. The skin depth is found with Equation 3.17, which takes the material resistivity into account. The resistivity for 843AR-340G is 2.2 $[\mu\Omega \cdot m]$ (MG Chemicals, 2022). The skin depth is calculated in Appendix B and provides a minimum thickness of 45.5 µm at the simulated resonance frequency, which is achieved by spraying multiple layers. The conductivity of the resin is very low, which reduces any eddy current. There are neither magnetic materials in the resin, which removes the challenge of hysteresis.

6.4.3 Unit cell structure

The first manufactured resonator was made as a conducting structure. This approach made the structure short-circuit itself whenever it was put under tension in the antenna frame. To avoid this problem, the resonator was manufactured again, but this time inverted into a sheet, as can be seen in Figure 6.6. The sheet was manufactured with SLA, painted with conductive spray and then sanded down. This approach decreased the surface of the

[5] https://www.mgchemicals.com/

resonator since it now became one-sided. The final results can be seen in Figure 6.7.

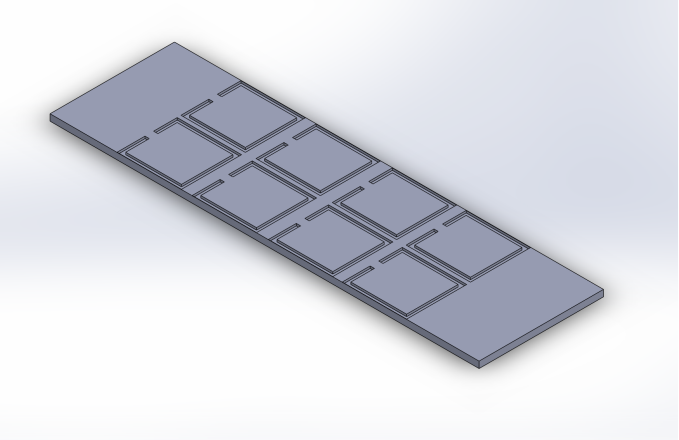

Figure 6.6: Metamaterial sheet modelled in Solid Works with C-ring resonators

Figure 6.7: Metamaterial sheet manufactured with resonators

6.4.4 Assembly

The parts were assembled with a probe feed, as illustrated in Figure 6.8 and pictured in Figure 6.9.

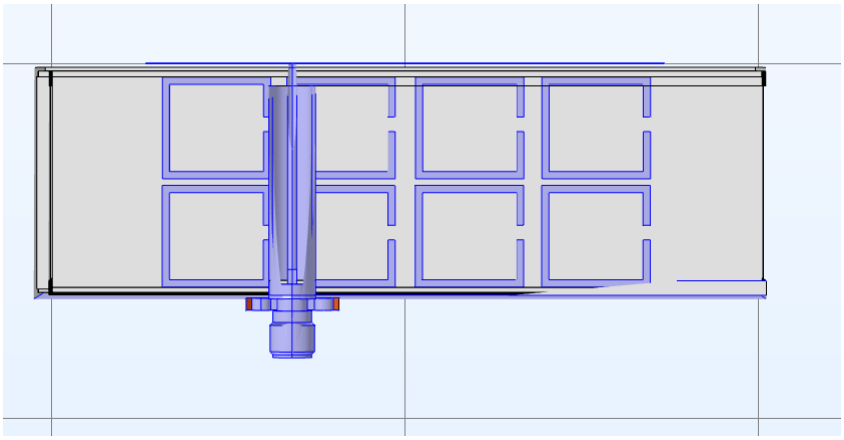

Figure 6.8: Metamaterial antenna crossection which shows the probe feed

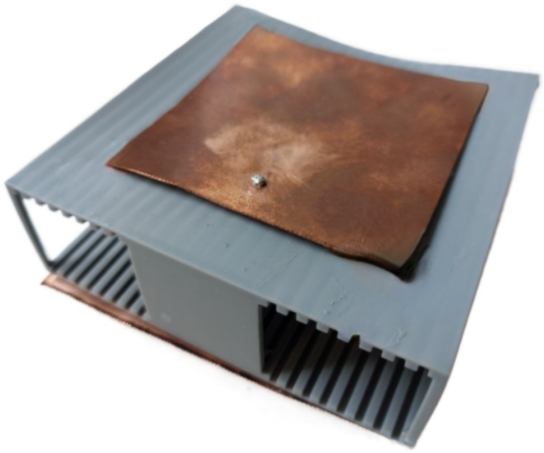

Figure 6.9: Metamaterial antenna frame with probe feed and no resonators. The top radiating patch and small ground are made from copper and glued to the Additive manufactured structure

6.5 Measurements

The University of Oslo has an anechoic chamber available for the measurement of antennas from 1 GHz and up. Tuning at the premises to minimize S_{11} reflections included moving the resonators slightly, as seen in Figure 6.11. The feed depth was also reduced to around 1.5 cm. An S_{11} plot was created, which according to Figure 6.10 had a minimum S_{11} reflection at 1.07 GHz. The measured S_{11} impedance frequency was very close to the minimum frequency of the anechoic chamber. This minimum frequency is determined by the dimensions of the chamber, the material and dimensions of the absorbing cones and the measuring equipment. Since the antenna operates close to the minimum frequency of the chamber, there could be some unwanted reflections in the room at these frequencies, which can create measurement errors in the final results. The manufactured antenna was mounted on top of two servo motors in the anechoic chamber and connected to a network analyser to extract the gain at spherical coordinates. Both the servo motors and the network analyser were remotely controlled by a computer, which allowed iterative rotation and measurements at each iteration. One servo motor rotated 360 ° while the other rotated up to 180 °. The antenna connector had been positioned rigidly under the ground plane, and due to its dimension, it needed an L-shaped SMA connector, which created a 90 ° displacement of the azimuth. The adjustment of the resonators and the positioning of the antenna mounted at an L-shaped connector is seen in Figure 6.11.

The second antenna in the anechoic chamber was a SAS-571 produced by A.H. Systems. It was a double-ridged guide horn antenna with a bandwidth from 700 MHz to 18 GHz. According to the vendor, it offers an average $VSWR$ under 2:1, linear polarization and a gain of up to 15 dBi. This double-ridged antenna is seen in Figure 6.12. The computer

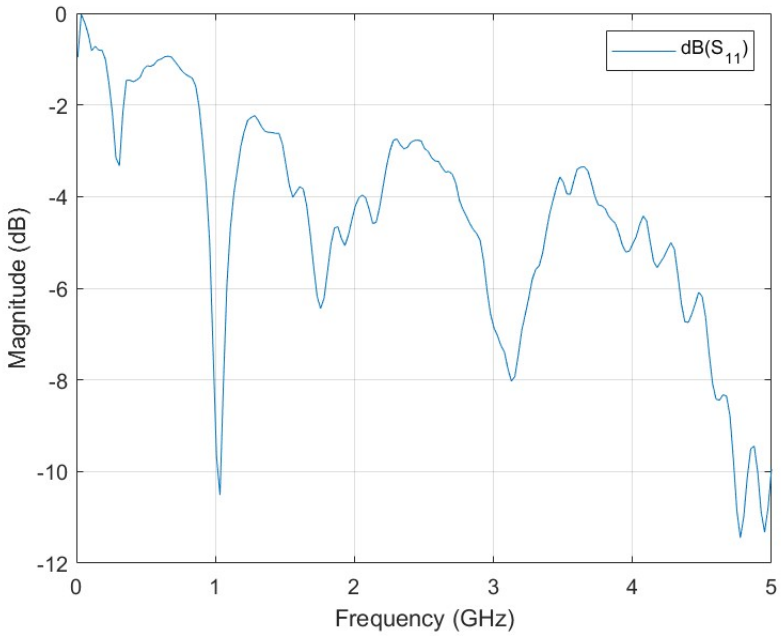

Figure 6.10: Metamaterial antenna measurements of S_{11} including C-ring resonators

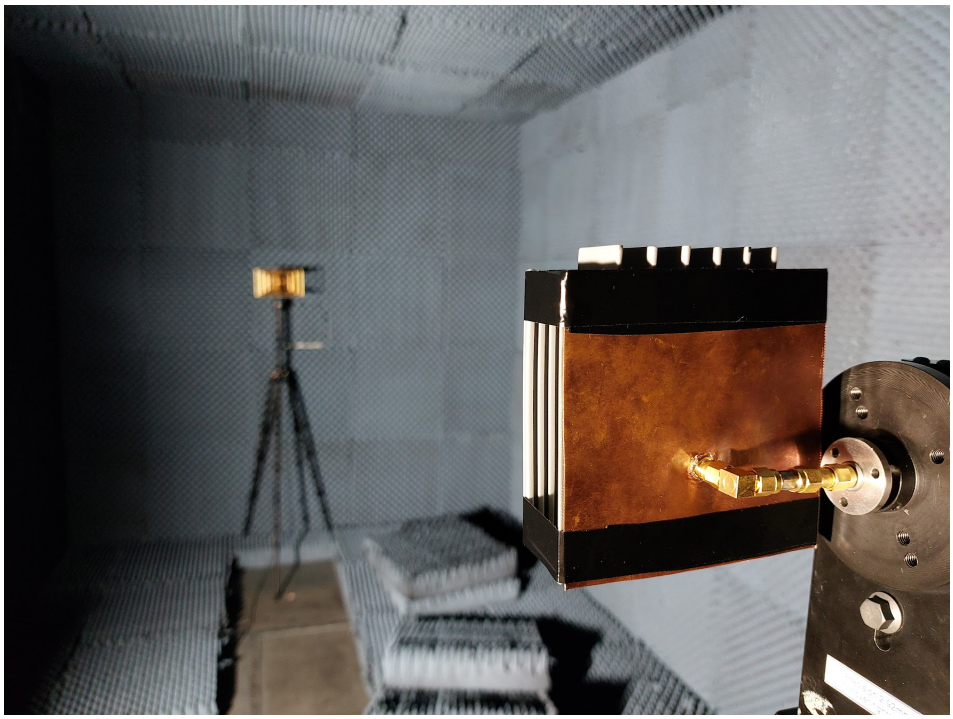

Figure 6.11: Metamaterial antenna in the anechoic chamber

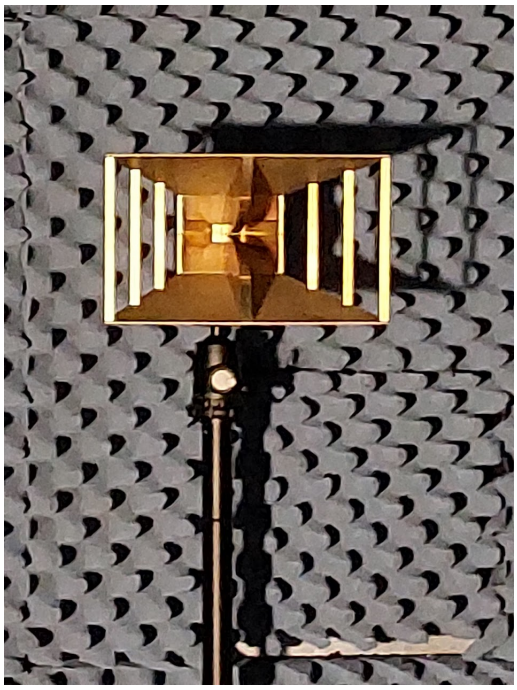

Figure 6.12: Second antenna in the anechoic chamber

was configured to record data at 5 ° iterations in all directions and at each iteration, the antenna measured gain and phase in the frequency range from 10 MHz and up to 5 GHz, with 35 MHz steps. The raw data was then set to compensate for both the path loss and radiation profile of the second antenna. The matrix with data was imported into MATLAB to generate plots.

The measurements of gain in the maximum direction are seen in Figure 6.13, and it shows the maximum gain to be at 0.983 GHz. Maximum gain is at a different frequency than the lowest measured S_{11}. One cause for deviation is the low accuracy when performing measurements with 35 MHz steps. When the incident energy in the -10 dB impedance bandwidth is neither reflected nor transmitted, it results in heat dissipation. The maximum gain is at the lower part of a -6 dB impedance bandwidth, where the energy is released as radiation. This could be due to the dispersion of the constitutive parameters, where only the lower part of the -6 dB impedance bandwidth is appropriately matched to the intrinsic far-field impedance. The measured maximum gain is in the lowest part of the frequency -range of the anechoic chamber, which may also have contributed to the deviation. The weak impedance match at resonance removes the possibility of recording any reasonable -10 dB impedance bandwidth, with a probe feed. However, the -6 dB impedance bandwidth was measured to 10.7%, which covers the frequencies with maximum gain.

At the frequency with maximum gain, it was created a plot of gain in all directions. This is seen in Figure 6.14, which shows a maximum gain of 2.3 dBi, with a small ground plane. The gain could improve if

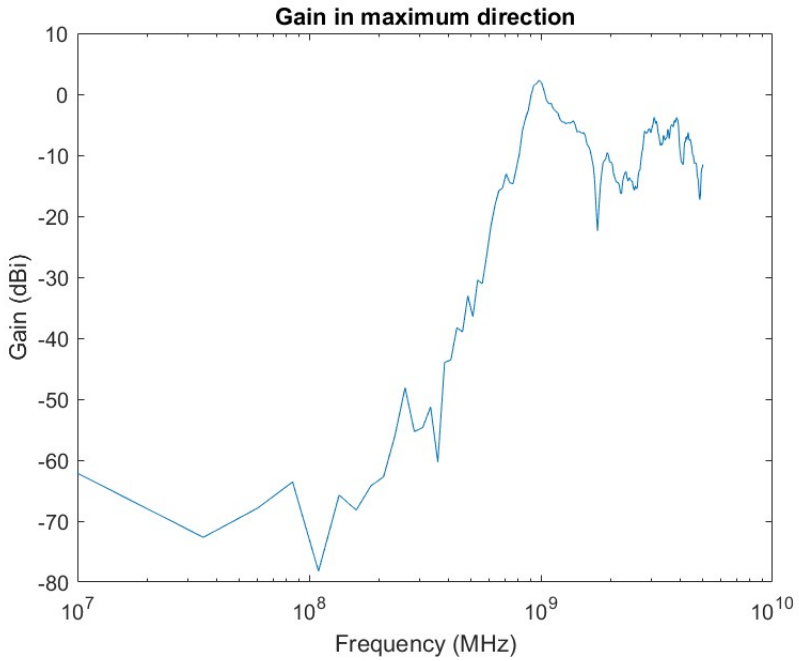

Figure 6.13: Measured gain from 10 MHz to 5 GHz with 35 MHz steps, in the direction of maximum gain at 0.983 GHz

the ground plane were enlarged, as was the case for the antenna with Magtrex 555. The average S_{21} over all directions at resonance is calculated to -5 dBi, in Appendix B. According to Equation 3.9, this will, relative to the maximum gain, suggests a maximum directivity of 7.3 dBi. The measurements resulted in two plots of gain with varying azimuth and elevation relative to gain in maximum direction, as seen in Figures 6.15 and 6.16. The plots indicate a half-power-beam-width around 105 ° and 90 °.

The measurements show the need for additional impedance matching, which could be achieved with an external matching network. Early prototyping proved that an inset feed at large heights resulted in large feed impedance which had degrading effect on the antenna performance. One hypothesis would be that an improved feed would also improve the radiation efficiency of the antenna. As a test, the patch was disconnected from the probe and separated with an isolating tape to achieve a capacitively coupled feed. This reduces the possibility of an improperly shielded feed probe resonating together with the patch. A capacitively coupled feed could then act as a series capacitance which reduced the overall capacitance. It was not time to measure the antenna again in an anechoic chamber after this modification. However, a test was performed with Wheeler's cap. A wavelength of 33 cm meets the manufactured Wheeler's cap minimum radius, which ensures most of the radiation to be reflected. However, there seemed to be low reflections at smaller wavelengths, which could be due to improper closing of the

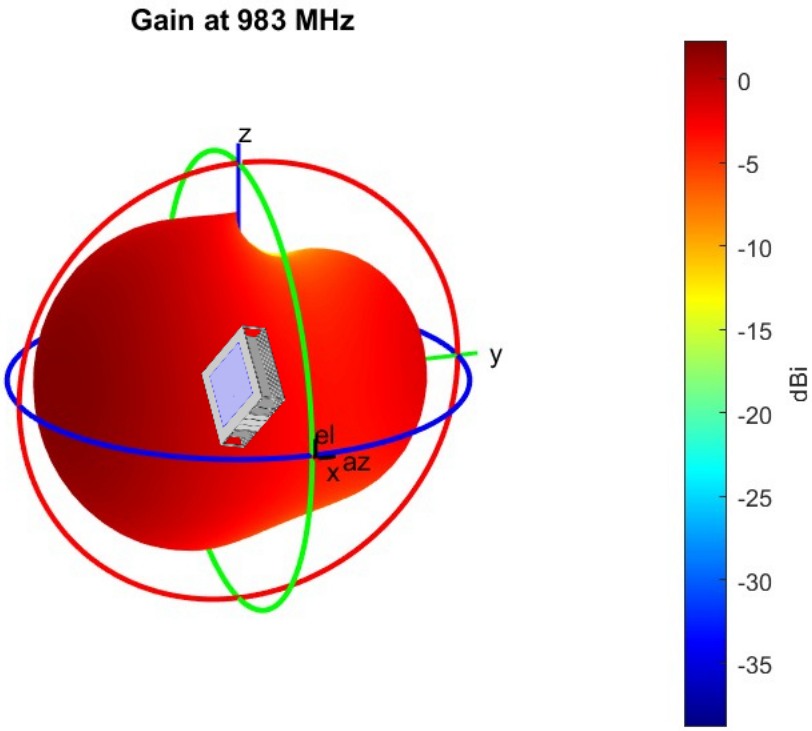

Figure 6.14: Measured three-dimensional model of the gain at 0.983 GHz

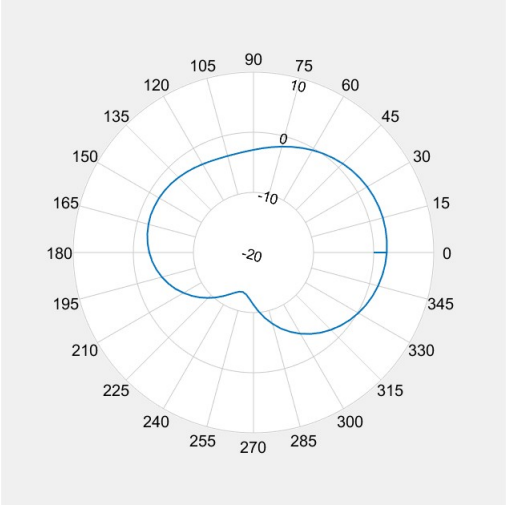

Figure 6.15: Measured gain for all angles of azimuth when elevation is set to the angle of maximum gain

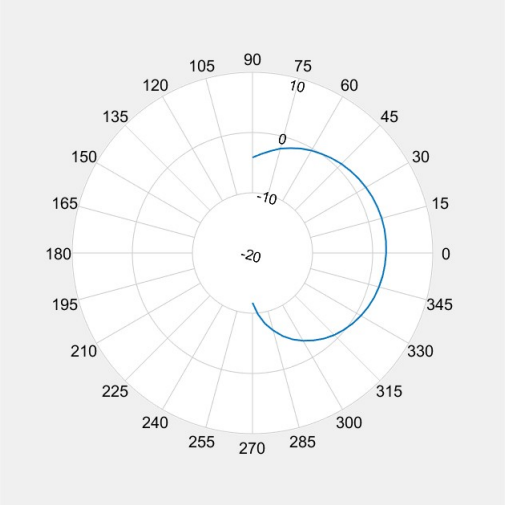

Figure 6.16: Measured gain for all angles of the elevation when azimuth is set to the angle of maximum gain

remaining gaps. Measurement of the S_{11} reflections at 1.02 GHz in free space was -18 dB, as seen in Figure 6.17, and within the cap, it was -4 dB, as seen in Figure 6.18. According to Equation 5.7 the radiation efficiency could now be calculated to 55% or -2.6 dB, which is a large improvement from the measurements in the anechoic chamber. Assuming a directivity of 7.26 dBi as measured in the anechoic chamber, this would result in a gain of 4.66 dBi.

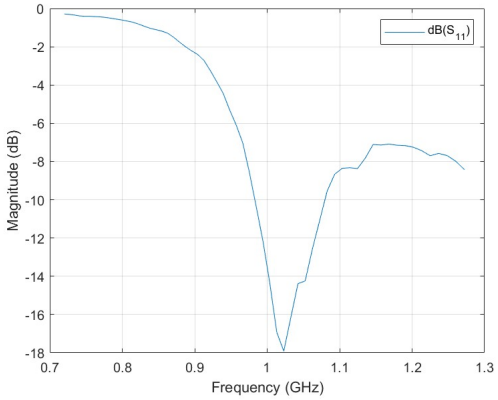

Figure 6.17: Measured improved S_{11} in free space after changing to capacitively coupled feed

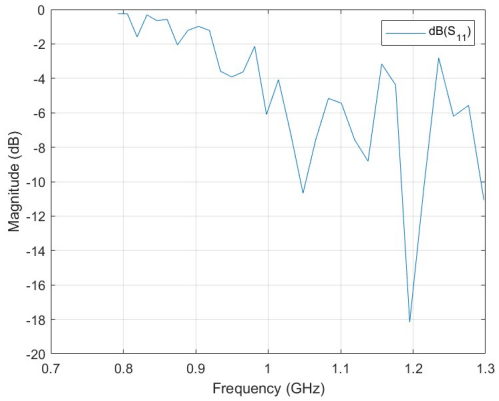

Figure 6.18: Measured improved S_{11} in a Wheeler's cap with capacitive coupled feed

Discussion

The deviation between measured resonance frequency with S_{11} and S_{21} indicates one or more design flaws either during simulation or manufacturing. Design flaws during the manufacturing process can be due to uneven cutting of ground and patch, design of feed or the creation of unit cells. Another reason for the deviation is the estimates which are utilized in the design process. Estimates have been utilized both for the resistivity of the conductors and for the dielectric properties of the resin.

The reduction of the resonance frequency is partly attributed to the large height of the antenna and following the length extensions. The calculated resonance frequency when taking the length extension from Equation 3.22 into account, is 1.57 GHz. This is visible in the simulated S_{11} plot in Figure 6.3, and was confirmed with measurement as a remaining very weak resonance at this frequency when the resonators were temporarily removed.

To understand how an improved patch dimension would affect the performance, S_{11} measurements were also performed with a decreased patch length. The result was a better match between the resonance frequency of the patch and the divergence frequency of the resonators, which resulted in a higher refractive index and an even higher miniaturization factor. However, this came at the cost of a worse impedance match and reduced radiation efficiency. Equally, when the length of the patch was gradually increased to approximate its natural half-wavelength dimension, the impedance match became gradually stronger as the resonance frequency increased.

Low radiation efficiency is accounted to a reduction of antenna volume (Ouedraogo et al., 2012). Harrington (1960) claimed that the gain is a result of the number of modes, as seen in Equation 3.16. Hence the gain could be kept high if the reduction of resonance frequency was compensated by a proportional increase of a matched refractive index. However, the manufactured antenna did not have a perfectly matching permittivity and

permeability.Alternatively, the resonator could have its diameter enlarged, which would eventually provide the resonator with matching relative permittivity and permeability at one and zero reduction of the resonance frequency. A second option would be if the resonator diameter was reduced to around 3.3 mm in diameter, where the negative permeability of 1.56 would match a positive permittivity of 1.56. This was not tested during the work of this thesis, but such a small diameter would require an even higher accuracy during the manufacturing process.

6.6 Summary

The metamaterial antenna measures minimum reflections at 1.07 GHz, which is close to the simulated minimum reflections at 1.04 GHz, which is a 55.7% reduction of the resonance frequency. A maximum gain of 2.3 dBi was recorded in an anechoic chamber with a probe feed, which is close to the gain of an omnidirectional antenna. The gain could be improved further, either by increasing directivity with a larger ground or with an improved impedance matching at resonance. During measurement in the anechoic chamber, it was due to low impedance match, not possible to record any -10 dB impedance bandwidth, but a -6 dB impedance bandwidth was measured to 10.7% which contains the frequencies with maximum gain. Then, a late modification to a capacitively coupled feed realized a 10% -10 dB impedance bandwidth and 55% radiation efficiency.

The low radiation efficiencies for the realized metamaterial antenna could be improved further. Even though adjustments to the design can be made, there will be limitations to the antenna gain based on the antenna dimensions (Harrington, 1960).

The antenna with metamaterials had the following properties after manufacturing;

- Square patch, which is 7.1 cm wide and has a 7.1 cm length
- Height of 3.3 cm
- Ground plane of 10x10 cm^2
- Maximum gain at 0.983 GHz with and a 10.7% -6 dB impedance bandwidth with a probe feed
- 55.7% reduction of resonance frequency
- Maximum gain of 2.3 dBi with probe feed, which should improve with coupled feed
- -10 dB impedance bandwidth at 10%, when switched to coupled feed
- 55% radiation efficiency was realized with coupled feed through measurements with Wheeler‘s cap

Chapter 7

Future work

7.1 Development of new magneto-dielectric materials

There exist many other promising magneto-dielectric materials which are created in laboratories but never commercialized. Some of them achieve both high matched refractive index and low loss tangents, and one example is the barium hexaferrite (Kim et al., 2014). The materials can be tailored to achieve even more promising characteristics by adjusting the material composition and grain size (Sistané, 2016). Based on their unique characteristics, the materials can be shaped and integrated into an antenna to make them physically small but still deliver in accordance with tailored requirements.

7.2 Unit cell design

The simulations in this thesis prove that the frequency response of the resonators is directly related to the length of its unwrapped conductor. More complex designs of the resonator could be utilized to achieve resonance at lower frequencies, as with the higher orders of the Hilbert fractal resonator. The resonators could be adjusted into a shape that is no longer square to reduce their height in a vertical orientation. Since the resonator is a two-dimensional conducting structure, the resonator does have an anisotropic effect on the antenna. As an alternative, three-dimensional resonators could provide isotropic behaviour.

7.3 Equations for antennas with magnetic substrates

There exists a plethora of equations which accurately predict the behaviour of a transmission line over a dielectric substrate. This includes equations for calculating the effective permittivity, optimal width of microstrip and its ideal feed position (Hammerstad and Jensen, 1980). However, both the permittivity and permeability affect the impedance of the antenna, and the equations which were found did not take magnetic materials into account. If the utilization of magnetic materials for antennas gains more traction in

the future, there will be a growing need for equations which also consider magnetic permeability. Another study (Niamien et al., 2011) claim that there is no available formula for calculating the effective permeability of a substrate.

7.4 Tailoring for specific use-case and optimizing the design

This thesis has not targeted any specific communication system, even though some alternatives was mentioned in section 3.7. Based on the specific use-case, the antenna should be tailored to requirements for reduction of resonance frequency, bandwidth, radiation efficiency, directivity and gain, to maximize its potential. Since impedance matching has been a challenge for the current design, the final antenna should also include an external matching network, before new measurements and utilization.

Chapter 8

Conclusion

This thesis has presented the design and measurements of two UHF microstrip antennas, which both included material-based reduction of the resonance frequency. Both antennas were simulated, measured and compared to a reference antenna with similar patch dimensions. Modelling and simulations were performed with COMSOL Multiphysics 6.1 [1], and measurements of -10 dB impedance bandwidth and gain were carried out in laboratories at the University of Oslo.

The first antenna included a magneto-dielectric substrate named MagTrex 555, which according to measurements, achieved a 76.6% reduction of the resonance frequency. A majority of the power was absorbed as magnetic losses, but due to high directivity with a large ground plane, the antenna is expected to realize a gain of 0.8 dBi. The measured -10 dB impedance bandwidth was 4.4%, which shows that magnetic materials provide a useful bandwidth even with a large reduction of the resonance frequency.

The second antenna was created with a metamaterial. The antenna was realized with Additive manufacturing ("3D printing") and measured in the anechoic chamber at the Institute for Informatics. The antenna offered a 55.7% reduction of resonance frequency, with a maximum gain of 2.3 dBi, even with a small ground plane. Due to poor impedance matching with a probe feed, it was not possible to record the -10 dB impedance bandwidth. However, a change to a coupled feed indicated a 10% -10 dB impedance bandwidth and a 55% radiation efficiency. A larger ground plane and improved design of the resonators, may enhance the antenna gain further.

The measurements support the simulated results, but it was difficult to measure optimal performance without an exact impedance match. The measurements were made with simple designs and commercially available materials, and the designs can be tailored for a vast variety of communications systems. Further experimentation would be needed to achieve the full potential of material-based reduction of the resonance frequency, with both natural and artificial magneto-dielectrics.

[1] http://www.comsol.com

References

Bae, S et al. (2009). 'Low loss Z-type barium ferrite (Co2Z) for terrestrial digital multimedia broadcasting antenna application'. In: *Journal of Applied Physics* 105.7, 07A515. DOI: 10.1063/1.3073940.

Balanis, C. A. (2005). *Antenna Theory Analysis and design, Third edition*. Hoboken, New Jersey: Wiley, 27–112, 231 and 811–843.

— (2012). *Advanced Engineering Electromagnetics*. New York: Wiley, pp. 39–57.

Chu, L. J. (1948). 'Physical Limitations of Omnidirectional Antennas Physical Limitations of Omnidirectional Antennas'. In:

Fallahpour, M. and R. Zoughi (2018). 'Antenna Miniaturization Techniques: A Review of Topology- and Material-Based Methods'. In: *IEEE Antennas and Propagation Magazine* 60, pp. 38–50.

Fujita, A., H. Kobiki and S. Gotoh (1998). 'Relationship between Residual Loss and Hysteresis Loss of MnZn Ferrites'. In: *Journal of the Magnetics Society of Japan* 22, pp. 286–288.

Gross, F. (Jan. 2011). *Frontiers in antennas: next generation design & engineering*.

Hammerstad, E. O. (1975). 'Equations for Microstrip Circuit Design'. In: pp. 268–272. DOI: 10.1109/EUMA.1975.332206.

Hammerstad, E. O. and O. Jensen (1980). In: *1980 IEEE MTT-S International Microwave symposium Digest*, pp. 407–409. DOI: 10.1109/MWSYM.1980.1124303.

Hansen, R. C. and Mary Burke (2000). 'Antennas with magneto-dielectrics'. In: *Microwave and Optical Technology Letters* 26.2, pp. 75–78. DOI: https://doi.org/10.1002/1098-2760(20000720)26:2<75::AID-MOP3>3.0.CO;2-W.

Harrington, R. (1960). 'Effect of antenna size on gain, bandwidth, and efficiency'. In: *Journal of Research of the National Bureau of Standards, Section D: Radio Propagation*, p. 1.

Ikonen, P. et al. (2006). 'On artificial magnetodielectric loading for improving the impedance bandwidth properties of microstrip antennas'. In: *IEEE Transactions on Antennas and Propagation* 54.6, pp. 1654–1662. DOI: 10.1109/TAP.2006.875912.

Kärkkäinen, Mikko and P. Ikonen (2005). 'Patch antenna with stacked split-ring resonators as an artificial magneto-dielectric substrate'. In: *Microwave and Optical Technology Letters* 46.

Kim, J. S. et al. (Jan. 2014). 'Effects of Magneto-Dielectric Ceramics for Small Antenna Application'. In: *Journal of Electrical Engineering and Technology* 9. DOI: 10.5370/JEET.2014.9.1.273.

Krzysztofik, Wojciech (June 2017). 'Fractals in Antennas and Metamaterials Applications'. In: ISBN: 978-953-51-3191-5. DOI: 10.5772/intechopen.68188.

Krzysztofik, Wojciech and Thanh Nghia Cao (2019). 'Metamaterials in Application to Improve Antenna Parameters'. In: *Metamaterials and Metasurfaces*. Ed. by Josep Canet-Ferrer. Rijeka: IntechOpen. Chap. 4. DOI: 10.5772/intechopen.80636. URL: https://doi.org/10.5772/intechopen.80636.

Li, J. et al. (Feb. 2019). 'Bi2O3 adjusting equivalent permeability and permittivity of M-type barium ferrite for antenna substrate application'. In: *Materials Research Express* 6. DOI: 10.1088/2053-1591/ab069c.

Litschke, O. et al. (2003). 'Adaption of the Wheeler-Cap method for measuring the efficiency of mobile handset antennas'. In:

Mathur, P. et al. (2010). 'Sustained electromagnetic properties of Ni-Zn-Co nanoferrites for the high-frequency applications'. In: *Materials Letters* 64.24, pp. 2738–2741. ISSN: 0167-577X. DOI: https://doi.org/10.1016/j.matlet.2010.08.056.

McLean, J. S. (1996). 'A re-examination of the fundamental limits on the radiation Q of electrically small antennas'. In: *IEEE Transactions on Antennas and Propagation* 44.5, pp. 672–. DOI: 10.1109/8.496253.

MG Chemicals (2022). *843AR Aerosol*. 5.7. MG Chemicals. URL: https://www.mgchemicals.com/downloads/tds/tds-843ar-a.pdf.

Niamien, C. et al. (2011). 'Compact Expressions for Efficiency and Bandwidth of Patch Antennas Over Lossy Magneto-Dielectric Materials'. In: *IEEE Antennas and Wireless Propagation Letters* 10, pp. 63–66. DOI: 10.1109/LAWP.2011.2107493.

Ouedraogo, Raoul O. et al. (2012). 'Miniaturization of Patch Antennas Using a Metamaterial-Inspired Technique'. In: *IEEE Transactions on Antennas and Propagation* 60.5, pp. 2175–2182. DOI: 10.1109/TAP.2012.2189699.

Pendry, J.B. et al. (1999). 'Magnetism from conductors and enhanced nonlinear phenomena'. In: *IEEE Transactions on Microwave Theory and Techniques* 47.11, pp. 2075–2084. DOI: 10.1109/22.798002.

Quiterio, G.-G. (2004). 'Patch-antenna efficiency based on Wheeler cap and measured Q factor'. In: *Microwave and Optical Technology Letters* 40.2, pp. 132–142. DOI: https://doi.org/10.1002/mop.11307.

Rogers Corporation (2019a). *Introduction to Magneto-Dielectric Materials for Antenna Miniaturization*. URL: https://www.youtube.com/watch?v=1VoMW8-Wo54.

— (2019b). *MAGTREX 555 High Impedance Laminates*. Rogers Corporation. URL: https://rogerscorp.com/-/media/project/rogerscorp/documents/advanced-electronics-solutions/english/data-sheets/magtrex-555-high-impedance-laminates-data-sheet.pdf.

Sistané, M. A. (2016). 'Permeability characterization of ferrites in the radio frequency range'. In:

Snelling, E. C. (1969). *Soft Ferrites, Properties and Applications*. Illiffe Books London.

Veselý, Petr et al. (Dec. 2018). 'Evaluation of dielectric properties of 3D printed objects based on printing resolution'. In: *IOP Conference Series: Materials Science and Engineering* 461, p. 012091. DOI: 10.1088/1757-899X/461/1/012091.

Walser, R. M. (2003). *Introduction to Complex Mediums for Electromagnetics and Optics*. Bellingham, WA, USA: SPIE Press.

Part I

Appendix

Appendix A

Extraction of data from COMSOL Multiphysics

COMSOL Multiphysics 6.1 with the RF module, was utilized for simulations. The geometry was set up together with the physics definition and the properties of the materials. Analysing the fields was then performed with a study which calculated the response over a frequency range, and provided standardized plots, such as S_{11}, Smith diagram and 3D and 2D normalized far-field radiation patterns.

Scattering parameter S_{11}

S_{11} was automatically plotted. It allows extracting the values as a table and plot the values with any third-party software.

Realized far-field gain

Realized far-field gain (emw.rGaindBEfar) is achieved by changing the expression for the plot of the far-field gain. The new plot also provides the maximum realized far-field gain and the maximum directivity.

Radiation efficiency

Power outflow over time average (emw.nPoav) was achieved by taking the surface average at the far-field sphere. The result is given in watt relative to a 1 W input. Similarly, the electromagnetic power loss density (emw.Qe) is extracted as a volume average over the whole substrate. This result is also given in watt relative to a 1 W input.

Surface current density

The surface current density is extracted with the normalized surface current density (emw.normJsdown), over the surface of the resonator of interest.

Magnetic flux density

The volume-averaged magnetic flux density (emw.normB) was extracted over all the domains.

Arrow plot of the electric and magnetic field intensities

The arrow plot is generated as a 3D plot with as a volume arrow. The expression was then set to the magnetic flux density (emw.Bx, emw.By and emw.Bz) and repeated again for the electric field (emw.Ex, emw.Ey and emw.Ez).

Appendix B

MATLAB calculations

FILE 1

```
%% init
clear all;
close all;
clc;

%% Physical constants
c = physconst('lightspeed'); %The speed of light in
   vacuum
mu_0 = 1.2566370614E-6; %The absolute permeability
epsilon_0 = 8.8541878128E-12; %The absolute
   permittivity
p=1/3.774E7; %Resistivity of aluminium suggested by
   COMSOL

%% Fixed design -parameter for all antennas
W=0.071 %Width of the antennas

%% FINDING THE ANTENNA PARAMETERS FOR THE REFERENCE
   ANTENNA
h_ref=(0.10-W)/6
er=1;
eeff=1;
f2_ref=c/(2*W)*(sqrt(2/(er+1)))
dL_ref = h_ref*0.412*((eeff+0.3)*(0.264+(W/h_ref)))
   /((eeff-0.258)*(0.8+(W/h_ref)))
L_real=W+dL_ref+dL_ref
f2_refext=300/L_real/2
L_ref=W

%Finding the feed depth
k = 2*pi*f2_ref/c;
```

```
fun1 = @(x) ((sin((k*W*cos(x))/2)/cos(x))^2)*(sin(x)
   .^3);
Ii = integral(fun1,0,pi);
G1 = Ii/(120*pi*pi);
fun2 = @(x) ((sin((k*W*cos(x))/2)/cos(x)).^2)*besselj
   (1,k*L_ref*sin(x)).*sin(x).^3;
G12 = integral(fun2,0,pi)/(120*pi*pi);
Rin = 1/(2*(G1+G12));
y0_ref = L_ref*(acos(sqrt(50/Rin)))/pi

%Finding the feed-width
B=(377*pi)/(2*50*sqrt(er));
wf_ref=h_ref*(2/pi)*(B-1-log((2*B)-1)+((er-1)/(2*er))
   *(log(B-1)+0.39-(0.61/er)))


%% FINDING THE ANTENNA PARAMETERS FOR THE NATURAL
   MAGNETO-DIELECTRIC ANTENNA
er = 6.588561538; %Relative permittivity of Magtrex
   555 at 370 MHz
Mu_r = 6.119846154; %Relative permeability of Magtrex
    555 at 370 MHz
mu = Mu_r*mu_0;
epsilon = er*epsilon_0;
tandm=0.053015385; %Loss tanget of Magtrex 555 at 370
    MHz
tande=0.012738462; %Loss tanget of Magtrex 555 at 370
    MHz
h_md=0.00254*4
eeff = ((er+1)/2)+((er-1)/2)*(1+12*(h_md/W))^-0.5;
f2_md = c/(2*W*sqrt(er*Mu_r))
dL_md = h_md*0.412*((eeff+0.3)*(0.264+(W/h_md)))/((
   eeff-0.258)*(0.8+(W/h_md)))
f2_mdext = 300/(W+dL_md+dL_md)/2
L_md = W;

%Finding the feed depth
k = (Mu_r*eeff)*2*pi*f2_md/c;
fun1 = @(x) ((sin((k*W*cos(x))/2)/cos(x))^2)*(sin(x)
   .^3);
Ii = integral(fun1,0,pi);
G1 = Ii/(120*pi*pi);
fun2 = @(x) ((sin((k*W*cos(x))/2)/cos(x)).^2)*besselj
   (1,k*L_md*sin(x)).*sin(x).^3;
G12 = integral(fun2,0,pi)/(120*pi*pi);
Rin = 1/(2*(G1+G12));
y0_md = L_md*(acos(sqrt(50/Rin)))/pi
```

```
%% FINDING THE ANTENNA PARAMETERS FOR THE
   METAMATERIAL ANTENNA
l=0.0145;
sep = 0.00065;
w = 0.0008;
t=0.0001;
h_meta=0.033;
Cellvolume=l*l*l*6;
Looparea=l*l;
file = "C:\Users\emanu\Dropbox\Master\1950Jmaxy4.txt
   ";
surfacecurrentfile = importdata(file, ' ', 5);
surfacecurrentvector=surfacecurrentfile.data(:,2);
file = "C:\Users\emanu\Dropbox\Master\1950B4.txt";
magneticfieldfile = importdata(file, ' ', 5);
magneticfieldvector=magneticfieldfile.data(:,2);
current = surfacecurrentvector.*l;
magnetizationvector=current.*Looparea./Cellvolume;
murvector=1./(1-magnetizationvector.*mu_0./
   magneticfieldvector);
frequencyvector=magneticfieldfile.data(:,1);
file = "C:\Users\emanu\Dropbox\Master\1950E4.txt";
electricfieldfile = importdata(file, ' ', 5);
electricfieldvector=electricfieldfile.data(:,2);
electricpolarizationvector=current./(1.*
   frequencyvector.*1000000);
permittivityvector=1+(electricpolarizationvector./(
   electricfieldvector*epsilon_0));
plot(frequencyvector(20:end),murvector(20:end))
hold on
plot(frequencyvector(20:end),permittivityvector(20:
   end))
xlabel('Frequency (MHz)')
ylabel('Permittivity(yellow) and Permeability(blue)')
hold off

er = 1.12; %Based on datadump
Mu_r = 2.79; %Based on datadump
n=sqrt(er*Mu_r);
eeff=er;

% Resonance frequency and the physical length
f2_meta = c/(n*2*W*sqrt(1))
L_meta = W;
dL_meta = h_meta*0.412*((eeff+0.3)*(0.264+(W/h_meta))
   )/((eeff-0.258)*(0.8+(W/h_meta)))
L_real=W+dL_meta+dL_meta
```

```
f_metareal=c/(2*L_real)

% Feed depth
k0 = 2*pi*f2_meta/c;
fun1 = @(x) ((sin((k0*W*cos(x))/2)/cos(x))^2)*(sin(x)
   .^3);
Ii = integral(fun1,0,pi);
G1 = Ii/(120*pi*pi);
fun2 = @(x) ((sin((k0*W*cos(x))/2)/cos(x)).^2)*
   besselj(1,k0*L_meta*sin(x)).*sin(x).^3;
G12 = integral(fun2,0,pi)/(120*pi*pi);
Rin = 1/(2*(G1+G12));
y0_meta = L_meta*(acos(sqrt(50/Rin)))/pi

%Required conductor thickness
Res843ar=2.2E-6;
delta=sqrt(Res843ar/(f2_meta*Mu_r*mu_0*pi))
Sigma=1/Res843ar;


OUTPUT

W =

    0.0710


h_ref =

    0.0048


f2_ref =

   2.1112e+09


dL_ref =

    0.0034


L_real =

    0.0777


f2_refext =
```

```
   1.9296e+03

L_ref =

    0.0710

y0_ref =

    0.0255

wf_ref =

    0.0238

h_md =

    0.0102

f2_md =

   3.3248e+08

dL_md =

    0.0043

f2_mdext =

   1.8838e+03

y0_md =

    0.0300

f2_meta =

   1.1943e+09
```

```
dL_meta =

    0.0183


L_real =

    0.1077


f_metareal =

   1.3923e+09


y0_meta =

    0.0279


delta =

   1.2932e-05
```

FILE 2

```
%% init
clear all;
close all;
clc;

%% Read file with gain from anechoic chamber and plot
    in 3D
file = "C:\Users\emanu\Downloads\metaant\
   metaant_gainxfer.txt";
metadata = importdata(file, ' ', 2);
figure
resample=2;
Resonancecollumn=81;
x=metadata.data(:,Resonancecollumn);
y=metadata.data(:,2);
z=metadata.data(:,1);
z=z-90; %Azimuth skew due to L connector
%p=PatternPlotOptions('MagnitudeScale',[1 1 1.5])
patternCustom(x,90-y,z);
title('Gain at 983 MHz');
```

```
h = colorbar;
ylabel(h, 'dBi')
Textdata = importdata(file, ' ', 1);
Frequencies = Textdata.data(1,1:end);
t=Frequencies((Resonancecollumn-1)/2);

%% Calculate average S21 and plot S21 over all
   frequencies in max gain direction
[MaxGain,index]=max(metadata.data(:,Resonancecollumn)
   );
Total=metadata.data(:,Resonancecollumn);
AverageGain=mag2db(sum(db2mag(Total))/2701)
Directivity=MaxGain-AverageGain
S21=metadata.data(index,3:resample:end);
figure
semilogx(Frequencies,S21)
title('Gain in maximum direction')
xlabel('Frequency (MHz)')
ylabel('Gain (dBi)')

%% Plot
XVertical=0;
YVertical=0;
n = 1;
while n < 2700
    if metadata.data(n,2)==metadata.data(index,2)
        XVertical(end+1)=metadata.data(n,
           Resonancecollumn);
        YVertical(end+1)=metadata.data(n,1);
    end
        n = n+1;
end

figure
polarpattern(YVertical,XVertical)
title('Gain measured for all angles of azimuth, when
   elevation is set to the angle of maximum gain.')


%% Plot
XHorizontal=0;
YHorizontal=0;

n = 1;
while n < 2700
    if metadata.data(n,1)==metadata.data(index,1)
        XHorizontal(end+1)=metadata.data(n,
           Resonancecollumn);
```

```
        YHorizontal(end+1)=metadata.data(n,2);

    end
        n = n+1;
end

figure
YHorizontal(1) = [];
XHorizontal(1) = [];
polarpattern(YHorizontal,XHorizontal)
title('Gain measured for all angles of the elevation,
    when azimuth is set to the angle of maximum gain.
   ')
```

OUTPUT

```
AverageGain =

   -4.9490


Directivity =

    7.2618
```